scientific reports

OPEN

Cholinergic-like neurons and cerebral spheroids bearing the PSEN1 p.Ile416Thr variant mirror Alzheimer's disease neuropathology

Nicolas Gomez-Sequeda, Miguel Mendivil-Perez, Marlene Jimenez-Del-Rio, Francisco Lopera & Carlos Velez-Pardo✉

Familial Alzheimer's disease (FAD) is a complex neurodegenerative disorder for which there are no therapeutics to date. Several mutations in presenilin 1 (PSEN 1), which is the catalytic component of γ-secretase complex, are causal of FAD. Recently, the p.Ile416Thr (I416T) PSEN 1 mutation has been reported in large kindred in Colombia. However, cell and molecular information from I416T mutation is scarce. Here, we demonstrate that menstrual stromal cells (MenSCs)-derived planar (2D) PSEN 1 I416T cholinergic-like cells (ChLNS) and (3D) cerebral spheroids (CSs) reproduce the typical neuropathological markers of FAD in 4 post-transdifferentiating or 11 days of transdifferentiating, respectively. The models produce intracellular aggregation of APPβ fragments (at day 4 and 11) and phosphorylated protein TAU at residue Ser^{202}/Thr^{205} (at day 11) suggesting that iAPPβ fragments precede p-TAU. Mutant ChLNs and CSs displayed DJ-1 Cys^{106}-SO_3 (*sulfonic acid*), failure of mitochondria membrane potential ($\Delta\Psi_m$), and activation of transcription factor c-JUN and p53, expression of pro-apoptotic protein PUMA, and activation of executer protein caspase 3 (CASP3), all markers of cell death by apoptosis. Moreover, we found that both mutant ChLNs and CSs produced high amounts of extracellular $eA\beta_{42}$. The I416T ChLNs and CSs were irresponsive to acetylcholine induced Ca^{2+} influx compared to WT. The I416T PSEN 1 mutation might work as dominant-negative PSEN1 mutation. These findings might help to understanding the recurring failures of clinical trials of anti-$eA\beta_{42}$, and support the view that FAD is triggered by the accumulation of other intracellular AβPP metabolites, rather than eAβ42.

Presenilin 1 (PSEN1) is an intramembrane aspartyl protease[1] which is the core of the γ-secretase complex responsible for amyloid-β (Aβ) generation[2,3]. Five PSEN1 mutations (e.g., p.Met146Leu, p.His163Arg, p.Ala246Glu, p.Leu286val, p.Cys410Tyr) were originally discovered in 1995 on human chromosome 14 (14q24.3) by genetic analysis of six large pedigrees with Alzheimer disease (AD)[4]. Since then, more than 300 mutations in PSEN1 have been reported (https://www.alzforum.org/mutations/psen-1) and are associated with the most common cause of early-onset familial Alzheimer's disease (FAD)[5]. Among those variants, the missense p.Glu280Ala (p.E280A) mutation was discovered in large Colombian kindred[6]. The PSEN1 p.E280A mutation of European ancestry[7], also known as the paisa mutation[8], affects nearly 1,000 individuals with about 400 confirmed carriers. Since the Colombian kindred has shown devoted participation and adherence in longitudinal studies, the effects of this mutation have been investigated extensively in connection not only with genetic[9,10], cellular[11–13], neuropathologic[14,15], neuropsychologic[16,17], and neurologic analyses[18–21] but also in biomarker progression[22–25] and prevention clinical trials (ClinicalTrials.gov Identifier: NCT01998841;[26]). Interestingly, the classical pathogenesis of the PSEN1 E280A mutation have been modeled in fibroblast-derived human induced pluripotent stem cells (hiPSCs)[11], in Warthon Jelly MSCs-derived cholinergic-like neuronal cells (ChLNs)[27], and in menstrual MSCs-derived cerebral spheroids (CSs)[28]. Specifically, the PSEN1 p.E280A ChLN cells and CSs displayed an

Grupo de Neurociencias de Antioquia, Instituto de Investigaciones Médicas, Facultad de Medicina, Universidad de Antioquia (UdeA), Calle 70 No. 52-21, and Calle 62 # 52-59, Torre 1, Laboratorio 412, Medellín, Colombia. ✉email: calberto.velez@udea.edu.co

increased secretion of extracellular Aβ, mostly eAβ$_{42}$ peptide fragment, intracellular aggregation of soluble amyloid precursor protein beta fragments (iAPPβf), oxidative stress (OS, i.e., oxidation of the stress sensor protein DJ-1 Cys^{106}SO$^-$ into Cys^{106}SO$_3$), loss of mitochondrial membrane potential (ΔΨ$_m$), hyperphosphorylation of the protein tau (at residue Ser^{202}/ Thr^{205}), dysregulation of intracellular Ca^{2+} influx, and apoptosis[27,28]. Although the exact mechanism by which PSEN1 (/γ-secretase) mutations generate high amounts of the extracellular amyloidogenic Aβ$_{42}$ fragment is not yet well-established[29–31], the PSEN1 p.E280A works as dominant-negative PSEN1 mutation[32,33], thereby triggering intracellular and extracellular Aβ-dependent signaling leading to neuronal death.

Unfortunately, in addition to the PSEN1 p.E280A mutation, 10 other PSEN1 mutations of European (five), Native American (three), undetermined (1), and African (one) ancestry have been reported in Colombia[34]. Specifically, a novel missense PSEN1 Ile416Thr (Chr14:73683951T > C; c.1247T > C; p.I416T) pathogenic variant of African ancestry that causes AD in large kindred has been reported in the Antioquia region[35] (for a journalistic version see[36]). Remarkably, the cerebral pattern of Aβ deposition and the PET-tau scans in I416T carriers resembled those previously reported in PSEN1 p.E280A carriers[37,38]. Likewise, neuropsychological evaluation of symptomatic carriers presented a mean age at onset of 42.35 ± 6.28 years for memory complaints, 47.6 ± 5.83 years for mild cognitive impairment (MCI), and the mean age of onset of dementia was 51.6 ± 5.03 years as well as depression, anxiety, delusions, hallucinations, and insomnia analysis also resembled those reported for the E280A mutation[8,39]. These observations suggest that both I416T and E280A are genetically and phenotypically homologous variants independently of their ancestry origin. However, whether the I416T variant expresses cellular and/ or molecular markers similarly to the E280A is still unknown. Answering this question is not a minor issue because this information might serve to answer whether potential treatment developments and/ or prevention clinical trials discovered in E280A might also apply to I416T patients. Furthermore, depending on the Aβ profiles generated by the different PSEN1 variants, it is possible to determine the pathogenicity of a particular mutation and predict age at disease onset[40]. Based on the above considerations, and the fact that both mutations are 100% penetrant[8,35], we posit that the I416T behaves molecularly like the E280A paisa mutation in cell models of FAD.

Endometrial mesenchymal stem cells (enMSCs) are a class of adult stem cells with self-renewal capacity, differentiation potential, low immunogenicity, low tumorigenicity, among other biological characteristics[41,42]. Specific surface markers (e.g., CD140b/ CD146 co-expression, SUSD2) have shown their perivascular identity in the endometrium, including the layer which sheds during menstruation. Cells with MSC properties have been identified in menstrual fluid and commonly termed menstrual blood stem/stromal cells (MenSC)[43]. Recently, we have validated MenSCs as a reliable source of planar (2D) ChLNs and cerebral spheroids (3D CSs) or neurospheres[44]. Since the protocol to obtain mutant hiPSCs take no less than 35 days[45,46], we selected PSEN1 I416T MenSCs as an experimental biological source, which presents minimal technical limitations, and minor ethical issues. Moreover, MenSCs-derived ChLNs and CSs display the AD neuropathological hallmarks by day 11[27,28]. In the present work, we aimed to establish an in vitro MenSCs-derived neuronal-like model bearing the mutation I416T. Like the E280A, we found that PSEN1 I416T mutation negatively affects the structure and functionality of MenSCs-derived planar (2D) ChLNs and 3D CSs expressing high iAPPβf aggregates and high amounts of eAβ$_{42}$, and hyperphosphorylated protein tau. Moreover, PSEN1 I416T also showed loss of ΔΨ$_m$, high production of reactive oxygen species (ROS, i.e., H$_2$O$_2$), signs of apoptosis death, and alterations in Ca^{2+} influx (Table 1). Therefore, we anticipate that experimental treatment approaches for FAD E280A[47] might be also valid for FAD I416T.

Results

Wild-type and PSEN1 I416T MenSCs differentiated into mesodermal and transdifferentiated into ectoderm lineages.

We first verified the genetic presenilin gene status of the MenSCs' donors. As shown in Fig. 1A, restriction fragment length polymorphism analysis (RFLP- VspI (AseI)) of a positive (control) heterozygous for the mutation PSEN1 I416T reveals three fragments of 560, 340, and 220 bp (track #1), whereas WT PSEN1 produces two fragments of 340, and 220 bp (track #2). The change of a T>C in codon 416 (i.e., ATT to ACT) generates a second cutting in the exon 11 of PSEN1 recognized by the restriction enzyme VspI (AseI). Based on this observation, we confirmed that the MenSCs sample (TBC# 45000) presents the PSEN1 I416T mutation (track #3). We also confirm that the DNA sample from a mutation carrier E280A (TBC#271) was negative for the PSEN1 I416T (track# 4). As a quality control, we incubated an aliquot of DNA with the

Condition > effect	Intracellular					Extracellular	Functionality
	iAPPβf	oxDJ-1 Cys^{106}	ΔΨ$_m$	CASP-3	p-TAU (Ser^{202}/ Thr^{205})	eAβ$_{42}$/eAβ40	[(Ca^{2+})$_i$]
E280A (2D)[#]	(↑)	(↑)	(↓)	(↑)	(↑)	(↑)	(↓)
E280A (3D)[$]	(↑)	(↑)	(↓)	(↑)	(↑)	(↑)	(↓)
I416T (2D)*	(↑)	(↑)	(↓)	(↑)	(↑)	(↑)	(↓)
I416T (3D)**	(↑)	(↑)	(↓)	(↑)	(↑)	(↑)	(↓)
WT*,**	(−)	(−)	(−)	(−)	(−)	(−)	(↑)

Table 1. Comparison of the effects of mutation E280A and I416T on cholinergic-like neural cells (2D) and on (3D) cerebral spheroids from human umbilical cord mesenchymal stromal cells (UC-MSCs) and human menstrual stromal cells (MenSCs). (↑) = increases; (↓) = reduces; (−) = no effect. [#]Ref.[27]. [$]Ref.[28]. *This work. **This work.

PSEN1 I416T mutation (TBC# 45000) without RE VspI (AseI) (track # 5, 540 bp band), or without DNA templates (or primers, Track# 6, no bands).

Since the MenSCs can differentiate into mesodermal and ectoderm cell lineages, we incubated WT and PSEN1 I416T MenSCs with their respective adipogenic, osteogenic, chondrogenic, and cholinergic medium according to standard protocols[44]. As expected, no differentiation markers were displayed in both WT and mutant MSCs when cultured in regular culture medium (RCm, Fig. 1B,D,F,H,J,L), whereas WT and mutant MenSCs differentiated into either osteocyte (Fig. 1C,E), adipocyte (Fig. 1G,I), or chondrocyte cells (Fig. 1K,M) according to osteocalcin, fatty acid binding protein 4 (FABP4), and aggrecan positive cells, respectively. Furthermore, MenSCs were also able to transdifferentiate into cholinergic-like neuronal cells (ChLNs, Fig. 1N–Q) according to cholinergic marker ChAT (Fig. 1R) and VAChT (Fig. 1S).

PSEN1 I416T ChLNs but not PSEN1 WT accumulates sAPPβf, induces loss of $\Delta\Psi_m$, shows oxidized oxidative sensor protein DJ-1, and high generation of reactive oxygen species (ROS). Next, we wanted to determine whether mutant neuronal-like cells express neuropathologic markers of AD. To this aim, we cultured ChLN cells for 0- and 4-days post-transdifferentiating in RCm. Then amyloid, mitochondria, OS markers were evaluated. As shown in Fig. 2, neither iAPPβf (Fig. 2A',B') nor oxidized DJ-1 protein (Fig. 2A",B") was detected in WT ChLNs at day 0 (Fig. 2A,E) and 4 (Fig. 2B,F), respectively. In contrast, I416T ChLNs show sAPPβf aggregates (Fig. 2C', D',E) and oxDJ-1 (Fig. 2C",D",F) at day 0 and 4 post-transdifferentiating (Fig. 2E,F). Indeed, the amount of iAPPβf and oxDJ-1 almost doubles at day 4 post-transdifferentiating. Flow cytometry analysis on day 4 (Fig. 2G–J) showed that the amount of sAPPβf and oxDJ-1 increased by +600% (Fig. 2G,H) and +384% (Fig. 2I,J), respectively compared to WT ChLNs. When the generation of ROS and $\Delta\Psi_m$ was evaluated in those cells, we found high $\Delta\Psi_m$ (Fig. 3A',B') but no ROS (Fig. 3A",B") in WT ChLNs by day 0 and 4 (Fig. 3A,B,E,F) according to immunocytochemistry analysis. The mutant ChLNs (Fig. 3C,D) show a significant reduction in $\Delta\Psi_m$ at day 0 (1.41-fold decrease, Fig. 3C',E) and at day 4 (1.10-f d, Fig. 3D',E), but a significant increase in ROS generation (2.25-fold increase and 3.0-f i, Fig. 3C",D",F). A similar trend of observations was obtained by flow cytometry on day 4 (Fig. 3G–J). Indeed, the $\Delta\Psi m$ in mutant cells diminished -86% (Fig. 3G,H), whereas ROS production increased +1067% compared to WT PSEN 1 (Fig. 3I,J).

PSEN1 I416T ChLNs express activated c-JUN and CASPASE-3. It is known that ROS/ H_2O_2 activate c-JUN, P53, pro-apoptotic PUMA, and CASPASE-3[48]. Unsurprisingly, immunocytochemistry analysis showed that WT ChLNs display neither activated c-JUN (Fig. 4A',B'), nor CASP-3 (Fig. 4A",B") at day 0 (Fig. 4A,E,F) and 4 (Fig. 4B,E,F). On the contrary, we detected activated c-JUN (Fig. 4C' and 4D'), and CASP3 (Fig. 4C",D") at day 0 (11.0-f i: 4E, and 9.36-f i: 4F, respectively) and at day 4 (Fig. 4D, 17.42-f i: 4E, 4.20-f i: 4F, respectively) in I416T ChLNs. Flow cytometry evaluation revealed similar tendency of data at day 4 (Fig. 4G–J). Notably, c-JUN (Fig. 4G,H), and CASP3 (Fig. 4I,J), increased their expression by +780%, and +620%, respectively in PSEN 1 I416T ChLNs when compared to WT ChLNs.

PSEN1 I416T ChLNs express activated PUMA and P53. Like c-JUN/ CASP3, we found that WT ChLNs display neither activated PUMA (Fig. 5A',B') nor P53 (Fig. 5A",B") at day 0 (Fig. 5A,E,F) and 4 (Fig. 5B,E,F) according to immunocytochemistry analysis. We detected activated PUMA (Fig. 5C',D'), p53 (Fig. 5C",D") at day 0 (Fig. 5C, 3.20-f i: E, and 4.50-f i: F, respectively), and at day 4 (Fig. 5D, 5.70-f i: E, and 23.21-f i: F, respectively) in I416T ChLNs. Notably, PUMA (Fig. 5G,H), and P53 (Fig. 5I,J) increased their expression by +940%, and +400%, respectively revealed by flow cytometry assessment at day 4 (Fig. 5G–J) in mutant ChLNs.

PSEN1 I416T ChLNs display hyperphosphorylated protein TAU (p-TAU). Intracellularly hyperphosphorylated protein tau (p-TAU Ser202/Thr205) is a classical pathological marker in AD (Neddens et al., 2020). Therefore, we evaluated whether mutant ChLNs present p-TAU. Fig. 6 shows that WT ChLNs displayed no p-TAU at day 0 (Fig. 6A,E) and 4 (Fig. 6B,E). Likewise, no p-TAU was almost undetected in I416T ChLNs at day 0 (Fig. 6C,E), but the phosphorylated protein was identified in mutant ChLNs at day 4 (76.11-f i, Fig. 6D,E). Of note, p-TAU was increased by +520% in I416T cells compared to WT ChLNs according to flow cytometry analysis (Fig. 6F,G).

PSEN1 I416T ChLNs secrete high amounts of eAβ42. The molar ratio of $A\beta_{42}$ over $A\beta_{40}$ is extensively used as a proxy indicator for the pathogenic effect of presenilin mutations. Fig. 7A shows that WT PSEN 1 ChLNs produced a basal level of $A\beta_{40}$ and $A\beta_{42}$, whereas PSEN 1 I416T ChLNs released a basal level of $A\beta_{40}$ but high amount of $A\beta_{42}$ (i.e., twice the amount of $A\beta_{40}$) at 4 days of post-transdifferentiating. Therefore, mutant PSEN 1 significantly increased the amount of $A\beta_{42}$ peptide (by +125%) compared to WT PSEN 1, resulting in a higher ratio of $A\beta_{42}$ (2.42-fold increase, Fig. 7B).

PSEN1 I416T ChLNs respond to ACh stimuli. A typical functional feature of neurons is that they respond to ACh-induced Ca^{2+} influx. We, therefore, investigated whether PSEN1 I416T ChLNs respond to ACh stimuli. To this aim, both WT and mutant PSEN1 ChLN cultures were exposed to ACh (1 mM final concentration). Fig. 8 shows that ACh induced an elevation of intracellular Ca^{2+} in WT PSEN1 ChLNs at day 0 (Fig. 8A,E, average fluorescence change ($\Delta F/F$) = 2.58 ± 0.22), and day 4 post-transdifferentiating (Fig. 8B,G, ($\Delta F/F$)=2.77 ± 0.14), with a mean duration of 10 s each (n = 20 ChLN cells imaged, N = 3 dishes) according to cytoplasmic Ca^{2+} responses to Fluo-3-mediated imaging (Fig. 8F,H). However, PSEN1 I416T ChLNs posed a reduced intracellular Ca^{2+} influx response to ACh treatment at day 0 (Fig. 8C,E, ($\Delta F/F$) =1.19 ± 0.12) and 4 (Fig. 8D,G, ($\Delta F/F$) =

Figure 1. (**A**) Agarose gel electrophoresis for the I416T mutation isolated from samples of mutation carriers. PCR products from blood samples were subjected to restriction endonuclease digestion analysis using AseI enzyme, resolved on 2% agarose gel electrophoresis, and visualized with red gel under ultraviolet illumination. The size of the amplicon was 560 bp. The 340 and 220 bp fragments correspond to the wild-type phenotype, and the 560, 340, and 220 fragments are for the mutant heterozygous phenotype. (M) Molecular weight marker; track (1) positive control with the I416T mutation (Code 2495); track (2) Wild phenotype negative control (Code 69,308); track (3) mutation carrier (Code 45,000); track (4) mutation carrier E280A (Code 271); track (5) control of digestion (Code 4500, without the AseI enzyme); track (6) PCR control (without template). The original gel is presented in Supplementary Fig. 1. (**B, D**) Osteocalcin negatively stained undifferentiated MenSCs grown on regular culture medium. (**C, E**) Osteocalcin positively stained osteoblasts differentiated from MenSCs. (**F, H**) FABP4 negatively stained undifferentiated MenSCs grown on regular culture medium. (**G, I**) FABP4 positively stained adipocytes differentiated from MenSCs. (**J, L**) Aggrecan negatively stained undifferentiated MenSCs grown on regular culture medium. (**K, M**) Aggrecan positively stained chondrocytes differentiated from MenSCs. Image magnification, 20x. The images represent 1 out of 3 independent experiments. (**N–Q**) MenSCs transdifferentiated into cholinergic-like neurons. WT PSEN1 and PSEN1 I416T MenSCs were cultured in a cholinergic differentiation medium as described in the Materials and Methods section for 7 days. Thereafter, WT PSEN1 and PSEN1 I416T ChLNs were left in regular culture medium (RCm) for 0 and 4 days. Then cells were double-stained with primary antibodies against ChAT (red fluorescence; **N'–Q'**) and VAChT (green fluorescence; **N"–Q"**). The nuclei are stained with Hoechst 33,342 (blue fluorescence; **N'''–Q'''**). (**R**) Quantification of ChAT fluorescence intensity. (**S**) Quantification of VAChT fluorescence intensity. The figures represent 1 out of 3 independent experiments. One-way ANOVA, post hoc test Šidák. Data are presented as mean ± SD (*$p < 0.05$; **$p < 0.01$; ***$p < 0.001$).

0.78 ± 0.25, mean duration of 10 s (n = 20 ChLN cells imaged, N = 3 dishes)) compared to WT PSEN1 ChLNs (Fig. 8F,H).

PSEN1 I416T MenSCs generate cerebral spheroids (CSs) displaying classical neuropathologic features of FAD.
We further investigated whether mutant MenSCs transdifferentiated into CSs and whether CSs can express the pathological markers of FAD. To this purpose, WT and mutant MenSCs were cultured in *Fast-N-Spheres* medium for 11 days[49]. As shown in Fig. 9, both WT and mutant MenSCs transdifferentiated into CSs (Fig. 9A–D), albeit with different cellular profiles. While WT CSs showed none of the amyloid (Fig. 9A'), oxidative stress (Fig. 9A"), p-TAU (Fig. 9C'), or apoptosis marker CASP-3 (Fig. 9C"), the I416T CSs expressed a significant increase in sAPPβf/Aβ aggregates (4.0-f, Fig. 9B',E), oxidized DJ-1 (8.85-f, Fig. 9B",F), p-TAU (10.55-f i, Fig. 9D',G), and CASP-3 (516.66-f i, Fig. 9D",H) compared to WT CSs (Fig. 9E–H). Additionally, WT CSs show functional mitochondria membrane integrity (Fig. 10A'), but mutant CSs displayed a significant decrease in the $\Delta\Psi_m$ (1.42-f d, Fig. 10B',C) compared to WT CSs.

PSEN1 I416T cerebral spheroids (CSs) respond to ACh stimuli.
We also tested whether CSs respond to ACh. Fig. 11 shows the response of WT versus mutant CSs when puffed with ACh (1 mM) and recorded for at least 40 s. WT CSs displayed a high transient increase in Ca^{2+} inward (Fig. 11A,C; ($\Delta F/F$) = 0.526 ± 0.02) with a mean duration of 10 s (n = 20 ChLN cells imaged, N = 3 dishes), whereas mutant CSs were almost irresponsive to ACh (Fig. 11B,C, ($\Delta F/F$)= 0.024 ± 0.01) with a similar mean duration of 10 s (n = 20 ChLN cells imaged, N = 3 dishes, Fig. 11D)).

PSEN1 I416T cerebral spheroids (CSs) secrete high amounts of $eA\beta_{42}$.
Lastly, we measure the ratio of $A\beta_{42}$ over $A\beta_{40}$ in CSs. As shown in Fig. 7C, mutant CSs produced a significant higher basal level of $A\beta_{40}$ (+2.27-fold) than WT, but PSEN 1 I416T CSs significantly generated more $A\beta_{42}$ (+6.18-f) than WT. The ratio of $A\beta_{42}$ over $A\beta_{40}$ clearly shows that mutant CSs generated more $A\beta_{42}$ (3.28-f) than WT CSs (1.21-f, Fig. 7D).

Discussion
The development of planar (2D) and tridimensional (3D) in vitro models such as immortalized and iPSCs cell lines, or organ-like models has greatly contributed to the understanding of the cellular and molecular neuropathophysiological features of AD[50–52]. However, they are expensive and time-consuming[45,46]. In the present study, we were able to reproduce the neuropathology of AD in MenSCs-derived PSEN1 I416T ChLNs in 2D and 3D (cerebral spheroids) in vitro in 11 days by using *Cholinergic-N-Run*[53] and *Fast-N-spheres* medium[49], respectively. We report for the first time that PSEN1 I416T ChLNs displayed the typical intracellular aggregation of protein Aβ (at day 7) and overproduction of $eA\beta_{42}$ (at day 11), p-TAU (at day 11), mitochondria damage (at day 11), OS (at day 7), and apoptosis (at day 11). Furthermore, PSEN1 I416T ChLNs but not WT ChLNs were irresponsive to ACh-induced Ca^{2+} inward signal (at day 11). Taken together these findings suggest that intracellular aggregation of Aβ and OS rather than extracellular Aβ are the earliest molecular events involved in neuronal-like cells loss in FAD. In agreement with post-mortem AD aged brain[54,55], in vitro[27,56] and in vivo studies[54,57–59], we found iAPPβf/Aβ aggregates in PSEN1 I416T ChLNs as early as 7 days of MenSCs transdifferentiating. This observation mirrors findings in PSEN 1 E280A[27]. However, the identity of the iAβ species is not yet fully determined. Indeed, investigators have identified either iAβ[42], iAβ[45][27], or iAPPβf[27], among other Aβ species[60,61]. These findings might be explained by the technique applied for its detection such as immunohistochemistry and immunofluorescence microscopy which uses antibodies against different Aβ conformations (e.g., 6E10, 4G8, anti-Aβ[45]). Interestingly, by using mass spectrometry analysis and immunofluorescence microscopy
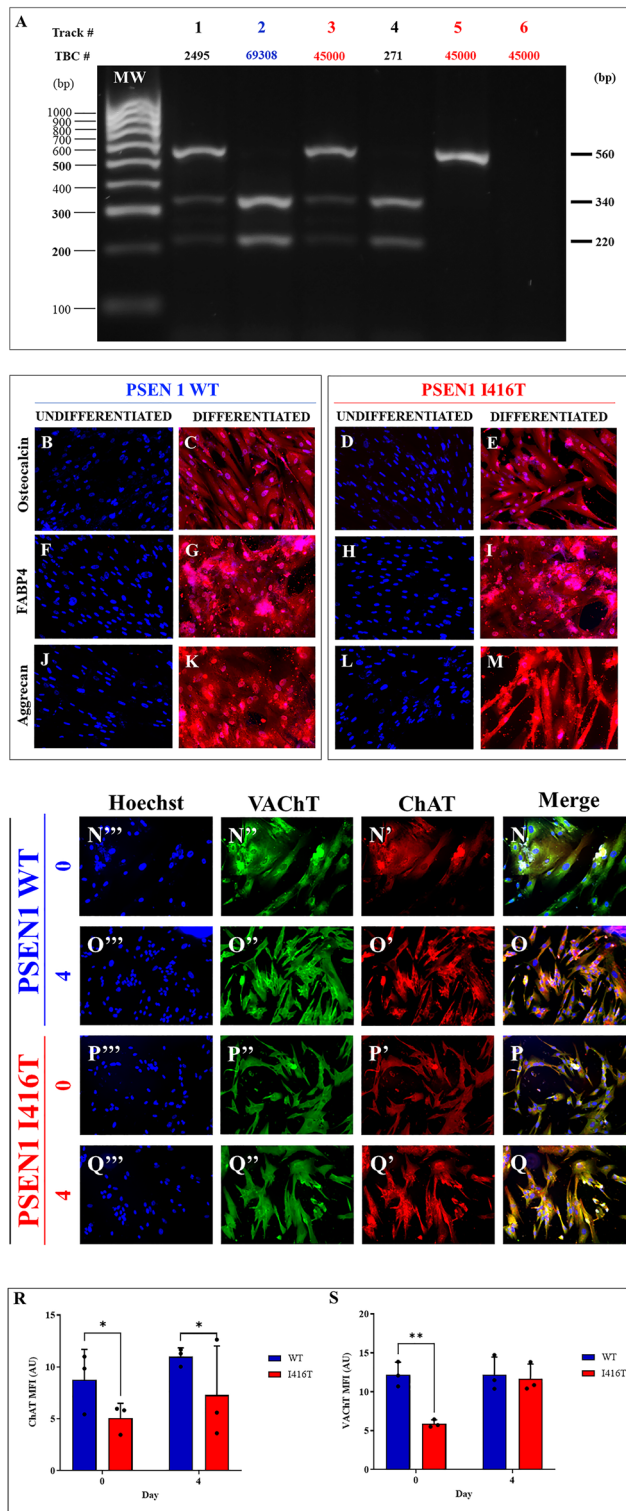
(6E10), we were able to identify several APP fragments (e.g., APP714, APP733, APP751, APP752, collectively named sAPPβf) but no $A\beta_{42}$ fragment was identified in PSEN 1 E280A ChLNs[27]. Whatever the true nature of Aβ, it accumulates intracellularly[54,62]. Like MSCs-derived PSEN 1 E280A ChLNs, we found intracellular APPβf accumulation in MenSCs-derived PSEN1 I416T ChLNs after 7 days of transdifferentiating (day 0). Interestingly, we also detected Aβ aggregates in PSEN 1 I416T CSs. These observations suggest that intracellular APPβ/Aβ fragments build up because full-length APP processing is altered and consequently some APP fragments remain intracellularly[63,64]. How exactly APPβf/Aβ is generated in PSEN 1 I416T (or E280A and other mutations) is still not yet fully understood. One possible explanation is that the processing of APP is a dynamic biologic process dependent on kinetic enzyme degradation, and cellular location of both β- and γ-secretases. In a normal neural cell, APP is sequentially cleaved by β-secretase (BACE1) freeing a soluble proteolytic fragment, recognized as
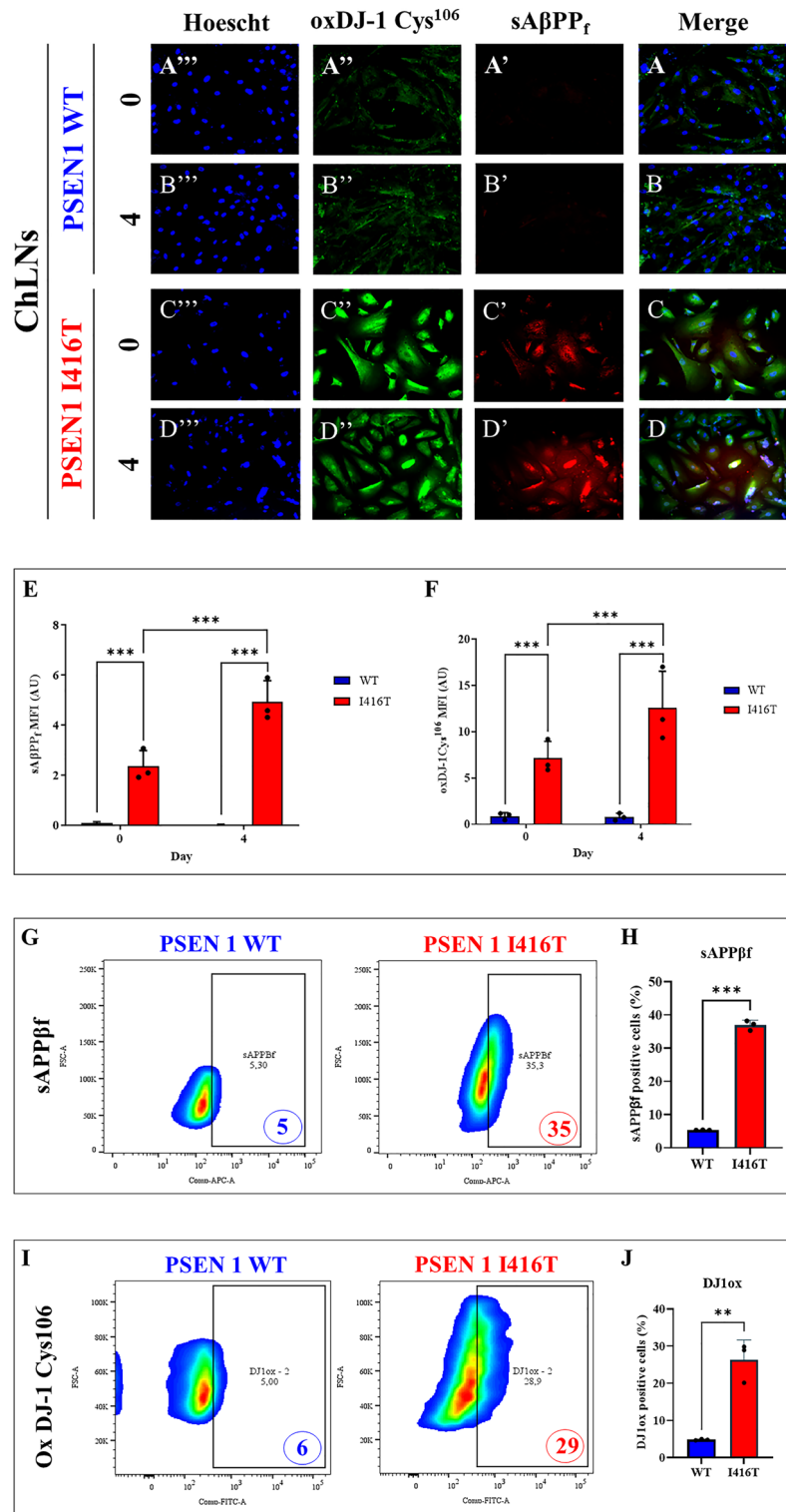
Figure 2. PSEN1 I416T Cholinergic-Like Neurons (ChLNs) show high levels of intracellular sAPPβf and oxidized DJ-1. WT PSEN1 and PSEN1 I416T MenSCs were cultured in a cholinergic differentiation medium as described in the *Materials and Methods* section for 7 days. Thereafter, WT PSEN1 and PSEN1 I416T ChLNs were left in regular culture medium (RCm) for 0 and 4 days. (**A–D**) Cells were double stained with primary antibodies against APP751/Aβ42 (red fluorescence; **A'–D'**) and oxDJ-1Cys^{106} (green fluorescence; **A"–D"**). The nuclei were stained with Hoechst 33,342 (blue fluorescence; **A'''–D'''**). (**E**) Quantification of sAPPβf by fluorescence intensity. (**F**) Quantification of oxDJ-1Cys106 fluorescence intensity (n = 3). (**G**) Quantification of sAPPβf by flow cytometry. (**H**) Quantification of sAPPβf by flow cytometry (n = 3). (**I**) Quantification of oxDJ-1 by flow cytometry. (**J**) Quantification of oxDJ-1 by flow cytometry (n = 3). Data are expressed as the mean ± SD; *$p < 0.05$; **$p < 0.01$; ***$p < 0.001$. The histograms and figures represent 1 out of 3 independent experiments. Image magnification, 200x.
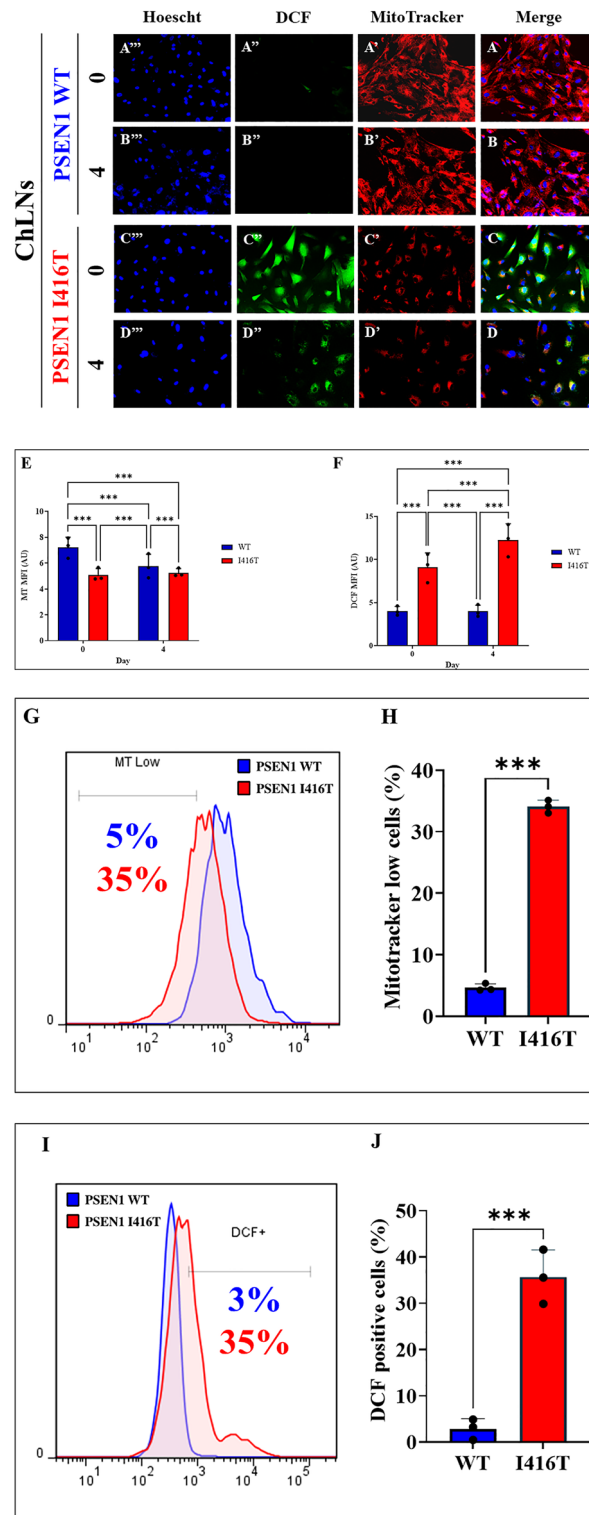
Figure 3. PSEN1 I416T Cholinergic-Like Neurons (ChLNs) show high mitochondrial membrane potential (ΔΨm), and high levels of intracellular reactive oxygen species (ROS). WT PSEN1 and PSEN1 I416T MenSCs were cultured in a cholinergic differentiation medium as described in the Experimental Procedure section for 7 days. Thereafter, WT PSEN1 and PSEN1 I416T ChLNs were left in regular culture medium (RCm) for 0 and 4 days. (**A–D**) Cells were double stained with MitoTracker™ Red FM (red fluorescence; **A'–D'**) and DCF (green fluorescence; **A"–D"**). The nuclei were stained with Hoechst 33,342 (blue fluorescence; **A'"–D'"**). (**E**) Quantification of ΔΨm by fluorescence intensity. (**F**) Quantification of DCF fluorescence intensity (n = 3). (**G**) Representative histogram showing ΔΨm by flow cytometry. (**H**) Quantification of ΔΨm by flow cytometry (n = 3). (**I**) Representative histogram showing DCF + by flow cytometry. (**J**) Quantification of DCF by flow cytometry (n = 3). Data are expressed as the mean ± SD; *$p < 0.05$; **$p < 0.01$; ***$p < 0.001$. The histograms and figures represent 1 out of 3 independent experiments. Image magnification, 200x.
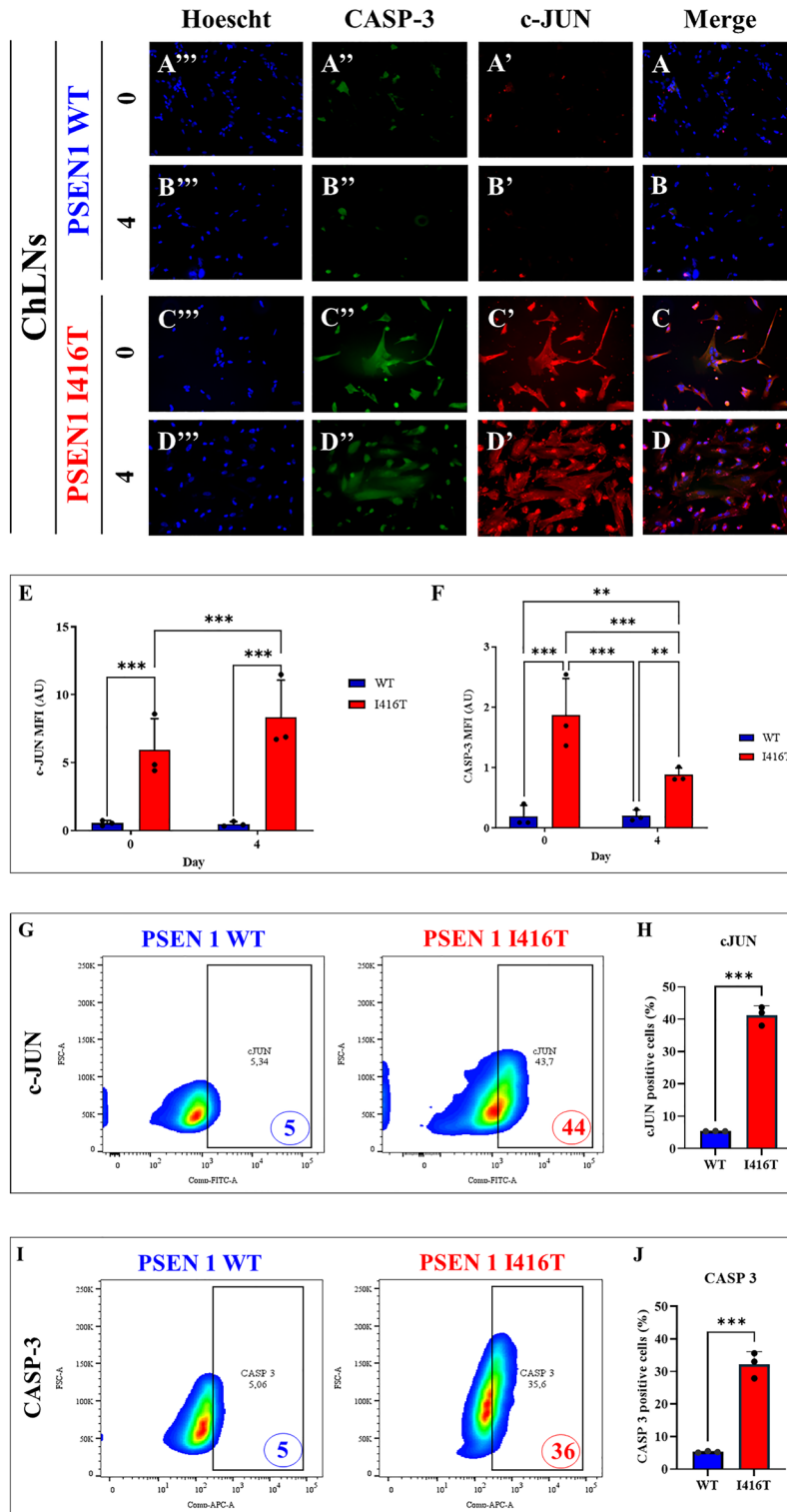
Figure 4. PSEN1 I416T ChLNs display activation c-JUN and CASPASE-3. WT PSEN1 and PSEN1 I416T MenSCs were cultured in a cholinergic differentiation medium as described in the *Materials and Methods* section for 7 days. Thereafter, WT PSEN1 and PSEN1 I416T ChLNs were left in regular culture medium (RCm) for 0 and 4 days. (**A–D**) Cells were double stained with c-JUN (red fluorescence; **A'–D'**) and CASPASE-3 (green fluorescence; **A''–D''**). The nuclei were stained with Hoechst 33,342 (blue fluorescence; **A'''–D'''**). (**E**) Quantification of c-JUN by fluorescence intensity. (**F**) Quantification of CASPASE-3 fluorescence intensity (n = 3). (**G**) Quantification of c-JUN by flow cytometry. (**H**) Quantification of c-JUN by flow cytometry (n = 3). (**I**) Quantification of CASPASE-3 by flow cytometry. (**J**) Quantification of CASPASE-3 by flow cytometry (n = 3). Data are expressed as the mean ± SD; *$p < 0.05$; **$p < 0.01$; ***$p < 0.001$. The histograms and figures represent 1 out of 3 independent experiments. Image magnification, 200x.
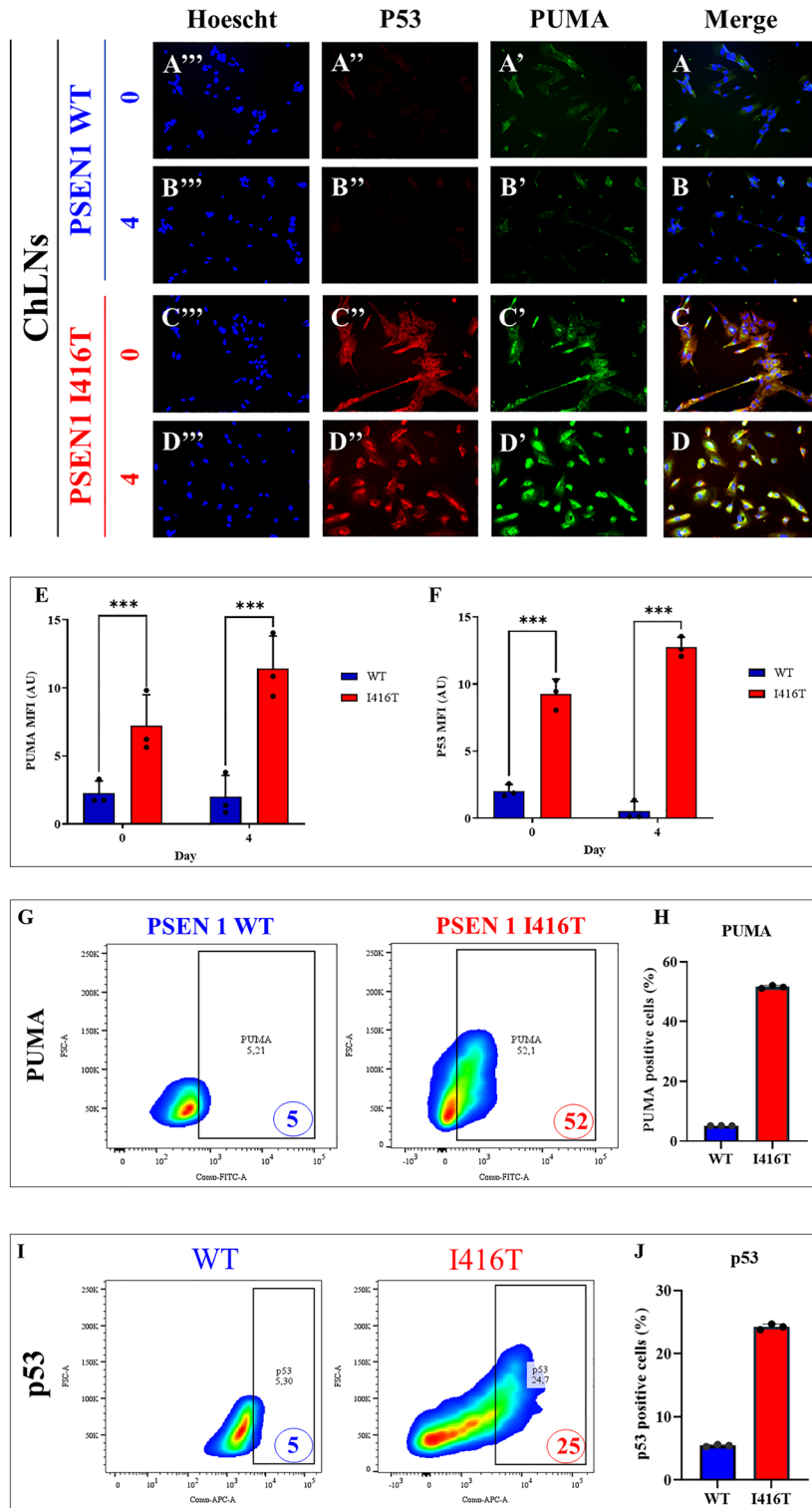
Figure 5. PSEN1 I416T ChLNs display activation P53 and PUMA. WT PSEN1 and PSEN1 I416T MenSCs were cultured in a cholinergic differentiation medium as described in the *Materials and Methods* section for 7 days. Thereafter, WT PSEN1 and PSEN1 I416T ChLNs were left in regular culture medium (RCm) for 0 and 4 days. (**A–D**) Cells were double stained with PUMA (green fluorescence; **A'–D'**) and P53 (red fluorescence; **A''–D''**). The nuclei were stained with Hoechst 33,342 (blue fluorescence; **A'''–D'''**). (**E**) Quantification of PUMA by fluorescence intensity. (**F**) Quantification of P53 fluorescence intensity (n = 3). (**G**) Quantification of PUMA by flow cytometry. (**H**) Quantification of PUMA by flow cytometry (n = 3). (**I**) Quantification of P53 by flow cytometry. (**J**) Quantification of P53 by flow cytometry (n = 3). Data are expressed as the mean ± SD; *$p < 0.05$; **$p < 0.01$; ***$p < 0.001$. The histograms and figures represent 1 out of 3 independent experiments. Image magnification, 200x.
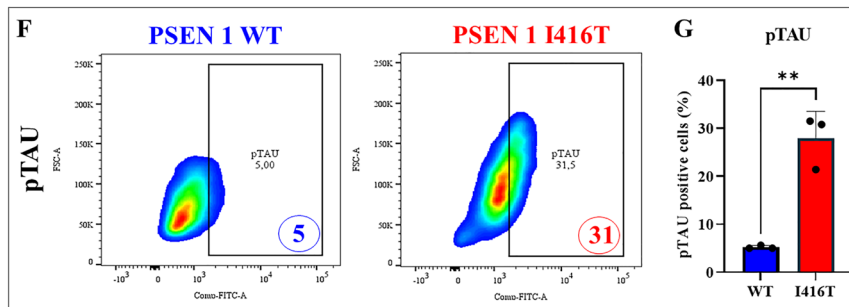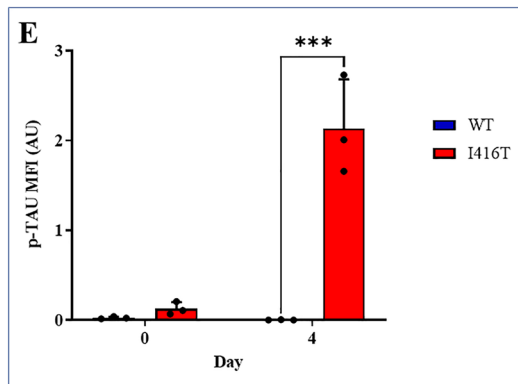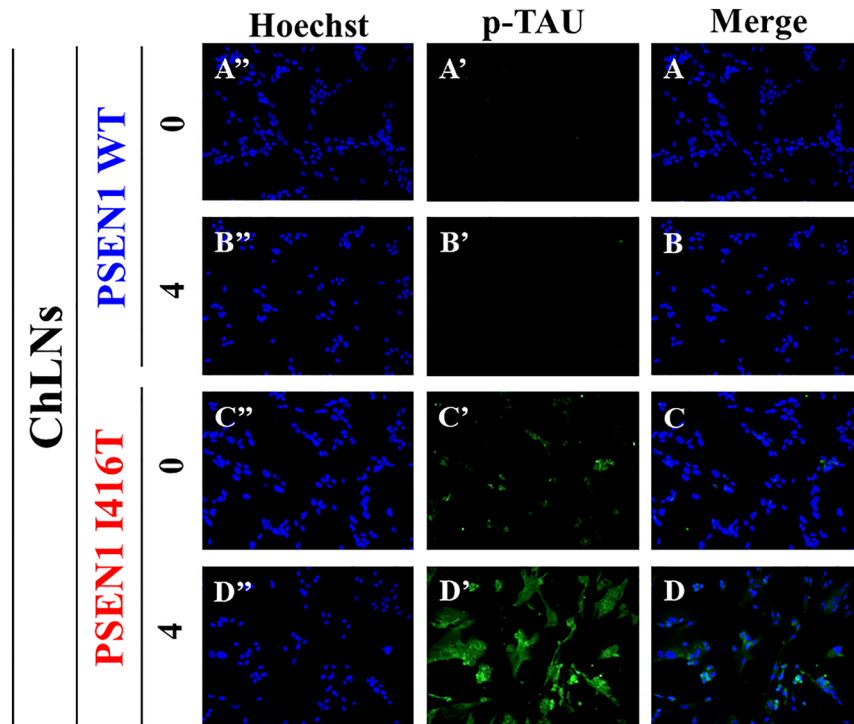
Figure 6. PSEN1 I416T ChLNs show high levels of phosphorylation of protein TAU. WT PSEN1 and PSEN1 I416T MenSCs were cultured in a cholinergic differentiation medium as described in the *Materials and Methods* section for 7 days. Thereafter, WT PSEN1 and PSEN1 I416T ChLNs were left in regular culture medium (RCm) for 0 and 4 days. (**A**–**D**) Cells were stained with p-TAU (green fluorescence; **A'**–**D'**). The nuclei were stained with Hoechst 33,342 (blue fluorescence; **A"**–**D"**). (**E**) Quantification of p-TAU by fluorescence intensity. (**F**) Quantification of p-TAU by flow cytometry. (**G**) Quantification of p-TAU by flow cytometry (n = 3). Data are expressed as the mean ± SD; *$p < 0.05$; **$p < 0.01$; ***$p < 0.001$. The histograms and figures represent 1 out of 3 independent experiments. Image magnification, 200x.
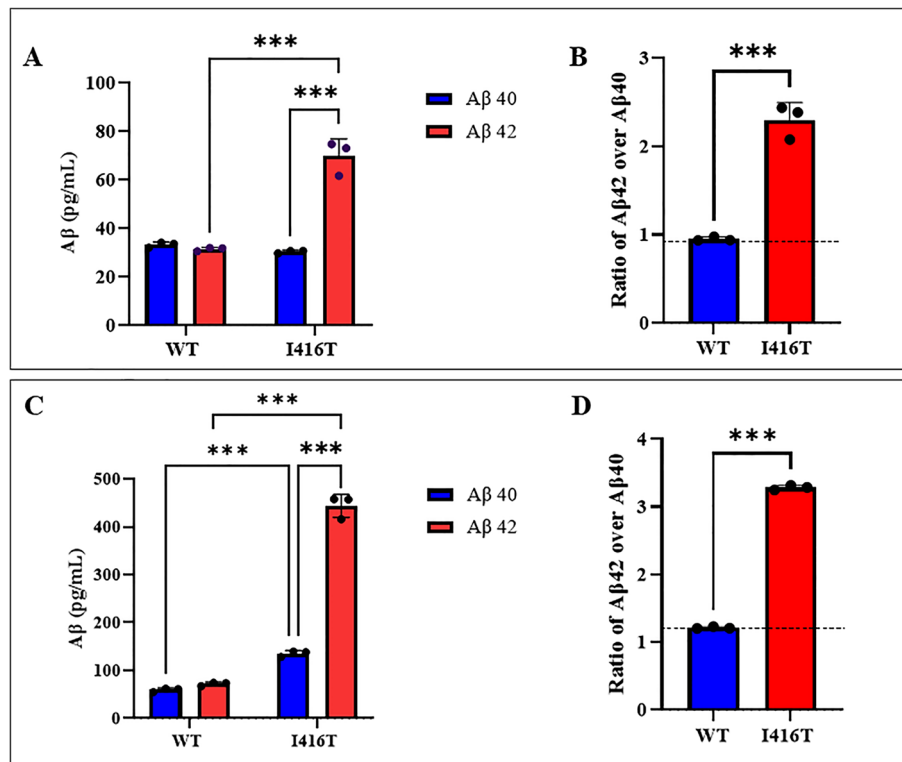
Figure 7. ELISA quantification of extracellular $A\beta_{40}$ and $A\beta_{42}$ peptide in supernatants from WT PSEN1 and I416T ChLNs and cerebral spheroids (CSs). WT PSEN1 and PSEN1 I416T MenSCs were cultured in a *cholinergic-N-Run* differentiation medium as described in the *Materials and Methods* section for 7 days. Thereafter, WT PSEN1 and PSEN1 I416T ChLNs were left in regular culture medium (RCm) for 4 days post-transdifferentiating. The levels of secreted $A\beta1-42$ and $A\beta1-42$ peptides were determined as described in *Materials and Methods* section. (**A**) ELISA measurements of supernatant from PSEN1 I416T ChLNs cells at day 4 post-transdifferentiating. (**B**) $A\beta42$ over $A\beta40$ ratio in PSEN1 I416T ChLNs compared with PSEN1 WT at day 4. WT PSEN1 and PSEN1 I416T MenSCs were cultured in a *Fast-N-Spheres* medium as described in the *Materials and Methods* section for 11 days. (**C**) ELISA measurements of supernatant from PSEN1 I416T CSs cells at day 11. (**D**) $A\beta42$ over $A\beta40$ ratio in PSEN1 I416T CSs compared with PSEN1 WT at day 11. The figures represent 1 out of 3 independent experiments. One-way ANOVA, post hoc test Bonferroni. Data are presented as mean $\pm$ SD (*$p < 0.05$; **$p < 0.01$; ***$p < 0.001$).

soluble APPβ (sAPPβ), which might be internalized and delivered to endosomes in the amyloidogenic pathway secreted extracellularly. The remaining C-terminal membrane-bound APP fragment, CTFβ or C99 fragment, undergoes additional cleavages by PSEN1/ γ-secretase to generate mainly $A\beta_{40}$ fragments (90%, nonamyloidogenic) and $A\beta_{42}$ (10%, amyloidogenic). The Aβ peptides are then secreted into the extracellular space when the endosome recycles to the cell surface[65]. In a mutant neural cell, APP is normally cleaved by BACE1 thereby generating APPβf, which by a still unknown mechanism, is stuck intracellularly, probably in early endosomes[66]. Since most mutations in PSEN1, including I416T / E280A, reduced γ-secretase enzymatic activity[33], it preferentially cuts at γ-site becoming into a major product line[67] overproducing $eA\beta_{42}$[68]. Furthermore, because I416T mutation might also be a trans-dominant negative mutation on γ-secretase[32,69], the APP-derived $eA\beta_{42}$ fragment might be a late event in the process of neuronal-like cell dismiss. Following this view, we detected early iAPPβf/iAβ (at day 7), and late $eA\beta_{42}$ (at day 11) in I416T 2D and 3D. Indeed, expression of the I416T mutation increased $A\beta_{42}$ levels but decreased $A\beta_{40}$ levels, resulting in overall increase in the $A\beta_{42}/A\beta_{40}$ ratio compared to those WT PSEN 1. Interestingly, it has been demonstrated that the PSEN1 L166P and G384A mutations cause re-localization of γ-secretase in MNT-1 cells (highly pigmented human melanoma cells), which significantly promotes the generation of intracellular long $A\beta_{42}$[70]. Therefore, our data suggest that PSEN 1 I416T mutation strongly enhances intraneuronal APPβf/Aβ aggregates in both ChLNs and CSs, thereby triggering a variety of intracellular signaling mechanisms leading to neuronal-like cell death. In agreement with others[71], these data suggest that iAPPβf/Aβ accumulation is the first step of a lethal cascade.

Previously, it has been shown that oxidation of the oxidative sensor protein DJ-1[106]-SOH (*thiolate*) into DJ-1[106]-SO₃ (*sulfonic acid*) by H_2O_2 and production of ROS were simultaneous events to the detection of Aβ aggregates in MSCs-derived PSEN 1 E280A ChLNs[27]. Here, we observed a similar phenomenon in both MenSCs-derived ChLNs I416T and CSs. However, the biochemical source of ROS/ H_2O_2 generated by APPβf/Aβ is not yet defined. Mounting evidence suggests that Aβ might interact with mitochondria, inducing disruption of the electron transport chain, thereby leaking electrons to oxygen, increasing ROS production, and H_2O_2[72]. Interestingly,
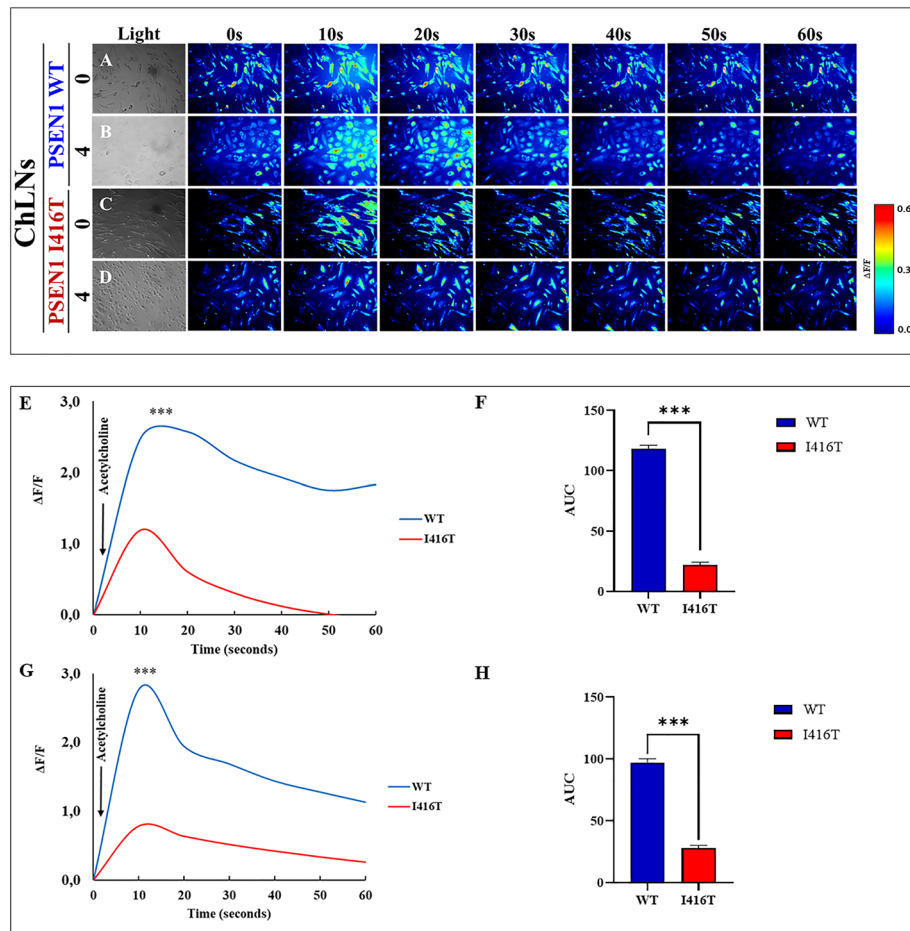
Figure 8. PSEN1 I416T ChLNs show a reduced functional response to Acetylcholine (ACh). After 7 days of transdifferentiating, WT PSEN1 and PSEN1 I416T ChLNs were left in regular culture medium for 0 and 4 days, as indicated in the figure. Time-lapse images (0, 10, 20, 30, 40, 60 s) of Ca^{2+} fluorescence in WT PSEN1 and PSEN1 I416T ChLNs after 0 (**A, C**), and 4 days (**B, D**) in response to ACh treatment. ACh was puffed into the culture at 0s (arrow). Then, the Ca^{2+} fluorescence of the cells was monitored at the indicated times. Color contrast indicates fluorescence intensity: dark blue < light blue < green < yellow < red. (**E, F**) Graph showing ΔF/F and area under the curve (AUC) of naïve and mutant cells in response to ACh treatment after 0 days. (**G, H**) Graph showing ΔF/F and area under the curve (AUC) of naïve and mutant cells in response to ACh treatment after 4 days post-transdifferentiating. The figures represent 1 out of 3 independent experiments. Data are expressed as the mean ± SD; $*p < 0.05$; $**p < 0.01$; $***p < 0.001$.

ROS (H_2O_2) production was high on day 0 than day 4 post-transdifferentiating, whereas loss of mitochondrial membrane potential and pathological markers expression was observed in day 4. These observations suggest that H_2O_2 generation is a cellular transient event (short-lived) and highly reactive towards other molecules via oxidative modification of critical redox-sensitive Cys (e.g., DJ-1)[73]. Once it has directly/ or indirectly activated target molecules including transcriptional factors (TFs), mitogen-activated protein kinases (MAPKs) and protein Tyrosine phosphatases[74,75], it fades away. Taken together these observations comply with the notion that H_2O_2 behaves as a second messenger[74,76]. In line with those findings, mitochondria-specific accumulation of amyloid-β/ H_2O_2 induces mitochondrial dysfunction leading to apoptotic cell death[77]. Effectively, we found that ChLNs I416T and CSs showed a significant loss of $\Delta\Psi_m$, and expressed several markers associated with regulated cell death. Indeed, ChLNs I416T displayed 2 important active pro-apoptotic transcription factors: c-JUN[78], and P53[79]. Interestingly, both c-JUN and P53 induce apoptosis by direct transcriptional activation of the pro-apoptotic BH3-only protein PUMA[80–82]. Once PUMA is up-regulated, it frames mitochondria to mitochondria outer membrane permeabilization (MOMP) allowing the release of pro-apoptogenic protein (e.g., cytochrome c) and activation of executer protein CASPASE-3[83]. As expected, PSEN 1 I416T ChLNs and CSs showed concurrent loss of $\Delta\Psi_m$ and overexpression of CASPASE-3, indicative of cell death by apoptosis. In agreement with others[57,84–86], our data suggest that APPβf/Aβ induces apoptosis in I416T ChLNs and mutant CSs. Despite overwhelming observations, other investigators have suggested that iAβ induces other modes of neuronal cell death such as oxytosis/ferroptosis[87], autophagy[88], and necrosis[89]. We, therefore, do not discard the possibility that I416T mutation might induce not only apoptosis but other supplementary cell deaths in ChLNs. However, further studies are necessary to enlighten this issue.
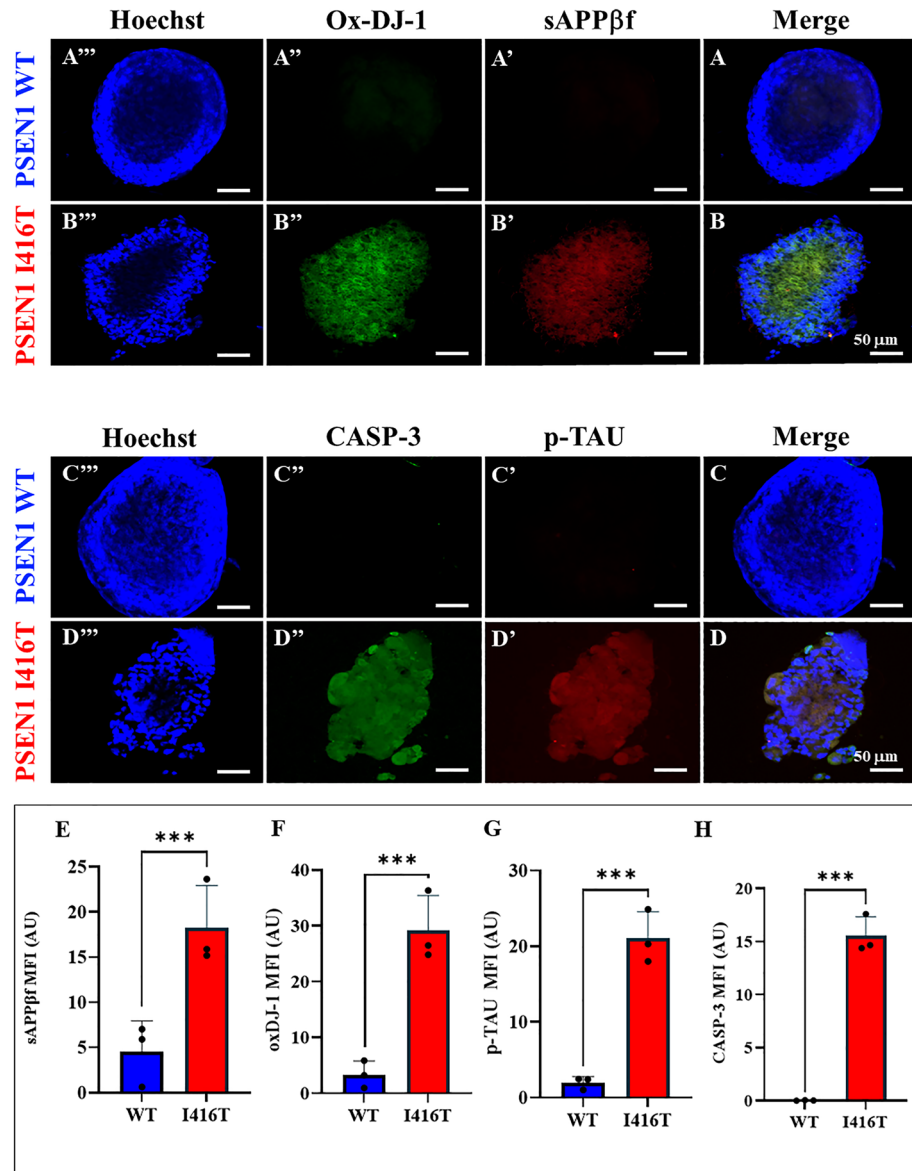
Figure 9. PSEN1 I416T Cerebral spheroids (CSs) show high levels of (i)sAPPβf, Ox-DJ-1, Tau phosphorylation (p-TAU) and caspase 3 (CASP3) activation. Both PSEN1 WT and I416T CSs were left in cultured for 11 days. Then, nuclei were stained with Hoechst (blue; A'''-D''') and CSs were double-stained as indicated in the figure with antibodies against Ox-DJ-1 (green; **A'',B''**), (i)sAPPβf (red; **A',B'**), CASP3 (green; **C'',D''**) and p-Tau (red; **C',D'**) and merged (**A–D**). Mean Fluorescence Intensity (MFI) quantification of iAPPβf (**E**), ox-DJ-1 (**F**), p-TAU (**G**), and CASP3 (**H**) reactivity from images obtained by immunofluorescence analysis of PSEN1 WT and I416T CSs. Significant values were determined by *Student's t-test*; ***$p < 0.001$. Image magnification 20x.

Hyperphosphorylation of protein TAU appears as a critical marker of neurodegeneration in AD[90]. Indeed, p-TAU at Ser^{202}/Thr^{205} is known to be increased in postmortem brains of AD[91], and p-TAU levels increases at later stages of AD[92]. We detected p-TAU (Ser^{202}/Thr^{205}) in both MenSCs-derived I416T ChLNs and CSs after 11 days of transdifferentiation but APPβf/Aβ aggregation at day 7. In agreement with others[93,94], our data suggest that APPβf/Aβ precedes p-TAU. A similar conclusion was reached with MSCs-induced PSEN 1 E280A ChLNs[27]. However, how exactly APPβf/Aβ triggers hyperphosphorylation of TAU is not yet established. One possibility is that APPβf/Aβ induces phosphorylation of TAU through c-JUN N-terminal kinase (JNK) signaling[95]. Since JNK can be phosphorylated and activated both pro-apoptotic protein c-JUN and TAU at (Ser^{202}/Thr^{205}), this kinase has become a potential therapeutic target[96].

Calcium fluxes are intimately involved in neuronal functionality[97]. Expectedly, neuronal calcium dyshomeostasis has been implicated in AD as disrupted Ca^{2+} could induce synaptic deficits and memory loss[98]. We found that both PSEN 1 I416T ChLNs and CSs were almost irresponsive to ACh-induced Ca^{2+} influx compared to WT ChLNs/ CSs. One possible explanation is that $eAβ_{42}$ might impair the interaction ligand-receptor by direct inhibition of alpha 7 nACh receptors[99]. Following this view, we found that PSEN 1 I416T ChLNs and CSs generated
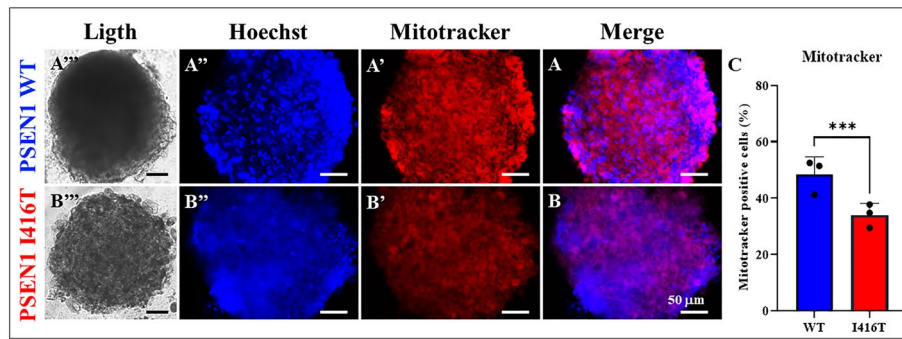
Figure 10. PSEN1 I416T Cerebral spheroids (CSs) show loss of mitochondrial membrane potential (ΔΨm). Both PSEN1 WT and I416T CSs were left in cultured for 11 days. Then, CSs (**A'''**,**B'''**) were double-stained as indicated in the figure with Hoechst (blue; **A''**,**B''**) and MitoTracker™ Red FM (red: **A'**,**B'**) and merged (**A**, **B**). (**C**) Mean Fluorescence Intensity (MFI) quantification of images obtained by fluorescence image analysis of PSEN1 WT and I416T CSs. Significant values were determined by *Student's t-test*; ***$p < 0.001$. Image magnification 20x.
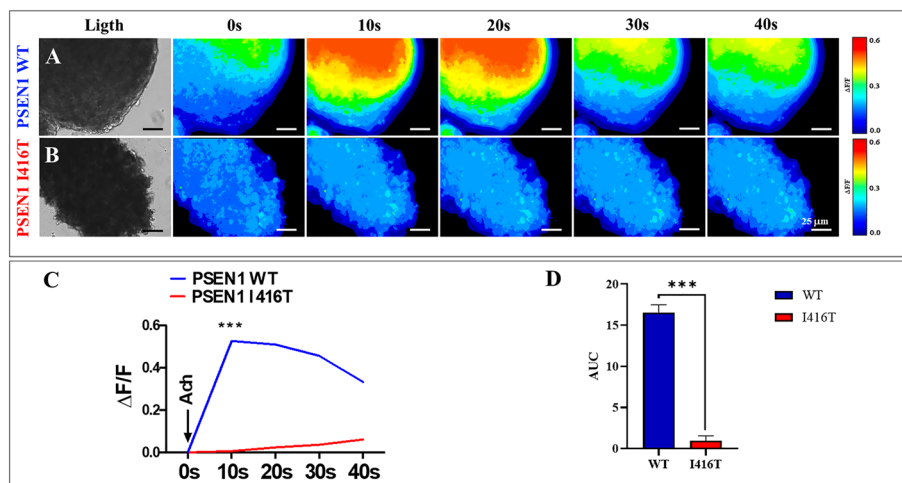

Figure 11. PSEN1 I416T Cerebral spheroids (CSs) show reduced functional response to acetylcholine (ACh). Both PSEN1 WT and I416T CSs were left cultured for 11 days. (**A**, **B**) Time-lapse images (Light, 0, 10, 20, 30 and 40 s) of Ca^{2+} fluorescence in CSs (n = 6 CSs imaged, N = 6 dishes) as a response to ACh treatment. ACh was puffed into the culture at 0 s (arrow). Then, the $Ca2+$ fluorescence of cells was monitored at indicated times. Color contrast indicates fluorescence intensity: dark blue < light blue < green < yellow < red. (**C**) Normalized mean fluorescence signal (ΔF/ F) over time, indicating temporal cytoplasmic Ca^{2+} elevation in response to ACh treatment in PSEN1 WT and I416T CSs. Significant values were determined by two-way ANOVA with a Tukey post hoc test; ***$p < 0.001$. Image magnification 20x.

high amounts of $eA\beta_{42}$. Although, the nature of AChRs in I416T neuronal-like cells are not yet known, the fast response of ChLNs to ACh-induced Ca^{2+} influx in WT neuronal-like cells suggests that WT and mutant ChLNs and CSs expressed pre-synaptic nAChRs[100]. Indeed, $eA\beta_{42}$ affects Ca^{2+} neuronal-like cells inwards. Therefore, acetylcholine receptor constitutes a potential therapeutic target for FAD.

Conclusion

The I416T is the second most frequent mutation in PSEN 1 in Colombia[34]. Interestingly, the clinical phenotype of this mutation resembles the clinical features of mutation PSEN 1 E280A, the most common mutation in the "Paisa" region[8]. Although neuropathological examination of postmortem brains and biochemical studies are still limited for the I416T, we demonstrate in vitro that PSEN 1 I416T MenSCs-derived ChLNs and CSs mirror the typical pathological features of sporadic AD and PSEN 1 E280A FAD[27] such as intracellular aggregation of APPβf, secretion of $eA\beta_{42}$, and phosphorylation of protein tau (Table 1). Although E280A and I416T mutations are structurally apart in the protein PSEN 1, our observations suggest that I416T also disables the catalytic action of PSEN 1/γ-secretase. However, whether the change of an isoline (hydrophobic residue) for a threonine amino acid (uncharged residue) at codon 416 disrupts the 3D structure of PSEN 1 as E280A does (acidic to hydrophobic residue)[30] needs further investigation. Whatever the structural change, I416T triggers iAPPβf aggregation, $eA\beta_{42}$, and p-TAU in ChLNs/ CSs irrespective of ethnic origin (e.g., African vs European (E280A)). Moreover, this

mutation causes OS and cell death by apoptosis in ChLN and CSs reflected by a significant increase in oxidation of sensor protein DJ-1, activation of pro-apoptotic protein c-JUN, and P53, expression of PUMA, and activation of executer protein CASP3. The present findings naturally mirrored for the first time the neuropathological features of FAD PSEN 1 I416T. Given that I416T resemble the pathological effects of E280A, and this last mutation decreased both $A\beta_{40}$ and $A\beta_{42}$ but the ratio $A\beta_{42}/A\beta_{40}$ favor $A\beta_{42}$[33], we anticipate that other PSEN-1 related mutation identified in Colombia (e.g., P117A, I143T, H163A)[34] might result in similar phenotypes as I416T/E280A mutations wherein there is an overproducing of iAPPβf in ChLNs or CSs. It would be interesting to test whether other mutations which produce $A\beta_{42}$ less than (e.g., D333G, T354I, N405S, A409T) or equal to WT PSEN 1 (e.g., I439V), or mutations with extremely high production of $A\beta_{42}$ (G384A)[33], are also alike to I416T phenotype. Given the origin of MenSCs, the present observations are limited to female gender. However, for confirmatory purposes, MSCs derived from male tissue (e.g., dental pulp, adipocyte tissue) should be included in future experimental settings. Further investigation is guaranteed on these issues. However, we consistently found iAPPβf in both as I416T/ E280A ChLNs as early as 7 days of transdifferentiating. These observations might contribute to the understanding of the recurring failures of clinical trials of anti-eAβ[101], and support the view that FAD is triggered by the accumulation of other intracellular APP metabolites, rather than eAβ42[102]. Therefore, other alternative treatment approaches should be pursued for FAD.

Methods

Isolation and characterization of menstrual stromal cells (MenSCs) derived from human menstrual blood (MB).
The present study was approved by University of Antioquia, Medellín, Colombia. The menstrual blood samples were collected from a healthy (Tissue Bank Code, TBC # 69308) and asymptomatic FAD (TBC #45000) female aged between 18 and 25 years. Donors provided a signed informed consent approved by the Ethics Committee of the Sede de Investigación Universitaria -SIU-, University of Antioquia, Medellín, Colombia (Act # 19–10-846). All experiments and/or experimental protocol/s were performed in accordance with relevant guidelines and regulations approved by University of Antioquia, Medellín, Colombia. Menstrual blood (MenB) was collected by cup collection (10–15 mL) during the first 3 days of menses. Briefly, menstrual blood samples were delivered into the laboratory and mixed with an equal volume of phosphate-buffered saline (PBS) containing 1 mM ethylenediamine tetra-acetic acid (EDTA), with 100 U/ml penicillin/streptomycin 0.25 mg/ml amphotericin B, and subject to cell lysis or standard Ficoll procedures within 24 h as previously described by[103]. After centrifugation, the cells suspended in a buffy coat ($7.7 \times 10^6 \pm 3 \times 10^6$ cells, n = 3) were transferred into a new tube, washed in PBS twice, and suspended in growth medium (low-glucose DMEM medium supplemented with 10% FBS (Gibco, USA), 100 U/ml penicillin/streptomycin 0.25 mg/ml amphotericin B) and seeded into 25 cm^2 plastic cell culture flasks at 37 °C with 5% humidified CO_2. The medium was replaced every 3 days leaving behind the adherent cells that were growing as fibroblastic cells in clusters. When the cells reached 80–90% confluence (passage 0, P0), the cells were detached by 0.25% trypsin/1 mM EDTA and sub-cultured to new flasks by the ratio of 1:3. The isolated MenSCs were evaluated for their differentiation capacity into an osteoblast, chondrocyte, and adipocyte lineage as well as for the presence of cholinergic-like neuronal markers (e.g., choline acetyltransferase, ChAT; vesicular acetylcholine transporter, VAChT) according to[53,104,105].

Identification of the PSEN1 I416T mutation in MenSCs.
The PSEN1 I416T mutation was detected by PCR using mismatch primers and digestion of the products with VspI (AseI isoschizomer) according to[35]. Digested products were separated on a 3% agarose gel. According to different mobility electrophoretic patterns, samples were classified as wild-type (WT, 340 and 220 bp bands) or mutant PSEN1 I416T (560, 340 and 220 bands) when compared to PSEN1 I416T carrier (positive DNA (control) case NeuroBank (NB) code #2495). The TBC #45,000 (female) sample was identified for PSEN1 I416T mutation, whereas TBC #69,308 (female) sample was identified for WT PSEN1. For comparative purposes, we included E280A PSEN1 DNA sample (TBC# 271) as an internal control.

Cell differentiation.
Osteogenic differentiation. Osteogenic differentiation was performed according to[104] with minor modifications. Briefly, WT and mutant MenSCs at passages 4–7 were plated at a density of 10,000 cells/ cm^2 in 12-well plates in a regular culture medium. After 72 h, the culture medium was replaced by osteogenic differentiation medium containing high-glucose DMEM (Sigma), 10% FBS, 1 μM dexamethasone (Alfa Aesar, cat # A17590), 250 μM sodium ascorbate (Sigma, cat # A4034), and 10 mM β-glycerophosphate (Alfa Aesar, cat # L03425). The medium was changed every 3–4 days. Control cells were kept in regular culture medium (RCm). After 20 days of induction, cells were fixed in 4% FA and incubated with the Mouse Anti-human osteocalcin monoclonal antibody (1:500; R&D, cat# MAB1419) followed by incubation with anti-mouse DyLight™ 594 secondary antibody (1:500) and 1 μM Hoechst 33,342 (Life Technologies).

Adipogenic differentiation. Adipogenic differentiation was performed according to[104] with minor modifications. Briefly, WT and mutant MenSCs at passages 4–7 were plated at a density 20,000 cells/cm^2 in a 12-well plate in a regular culture medium. At 90–100% confluence, the culture medium was replaced by adipogenic induction medium, including high-glucose DMEM, 10% FBS, 0.5 mM 3-isobutyl-1-methylxanthine (Sigma, cat # I5879), 100 μM indomethacin (Sigma, cat # I7378), 0.1 μM dexamethasone and 10 μg/ mL insulin. Control cells were kept in regular culture medium. After 20 days of induction, cells were fixed in 4% FA and incubated with the goat anti-mouse fatty acid-binding protein 4 (FABP4) antigen affinity-purified polyclonal antibody (1:500; R&D, cat# AF3150), followed by incubation with anti-goat DyLight™ 594 secondary antibody (1:500) and 1 μM Hoechst 33,342 (Life Technologies).

Chondrogenic differentiation.   Chondrogenic differentiation was performed according to[105] with minor modifications. Briefly, 5×10^4 WT and mutant MenSCs were left aggregated in microwell plates and then provided with chondrogenic medium containing high-glucose DMEM, 10% FBS, 10 µg/ L TGF-β3, 0.1 µmol/ L dexamethasone, 50 µmol/ L vitamin C, and 6.25 mg/L insulin. The medium was changed every 3–4 days. Control cells were kept in a regular culture medium. After 20 days of induction, cells were fixed in 4% FA and incubated with the goat anti-human aggrecan antigen affinity-purified polyclonal antibody (1:500; R&D, cat# 967,800) followed by incubation with anti-goat DyLight™ 594 secondary antibody (1:500) and 1 µM Hoechst 33,342 (Life Technologies).

Cholinergic-Like Neurons (ChLNs) differentiation.   The MenSCs were seeded at $1.6–2 \times 10^4$ cells/ cm² in 25 cm² culture flasks for 24 h in regular culture medium. Then, the medium was removed and cells were incubated either in minimal culture medium (MCm) or cholinergic differentiation medium (*Cholinergic-N-Run* medium containing DMEM/F-12 media 1:1 Nutrient Mixture Gibco (cat# 10,565,018, 10 ng/ mL), basic fibroblast growth factor (bFGF) recombinant human protein (Gibco cat# 13,256,029), 50 µg/ mL sodium heparine (Sigma-Aldrich cat# H3393), 0.5 µM all-trans retinoic acid, 50 ng/ mL sonic hedgehog peptide (SHH, Sigma cat# SRP3156) and 1% FBS) at 37 °C for 0, and 4 days according to[53].

Cerebral Spheroids (CSs) formation.   MenSCs were seeded at a density of 1.5×10^4 cells/cm² in a multi-well plate (Greinner-Bio-one, cat# 662102) using *Fast-N-spheres* medium (DMEN F-12 GIBCO®, cat#11,330–032; supplemented with 2% B27® GIBCO® (cat #17504-044), 20 ng/ml basic fibroblast growth factor (bFGF, R&D Systems, Inc., MN), 20 ng/ml epidermal growth factor (EGF, Sigma cat#E9644), 1 µg/ml heparin sodium salt®, and 100 U/ ml penicillin/streptomycin for 11 days according to[49]**.**

Immunofluorescence analysis.   For the analysis of neural-, Alzheimer disease-, oxidative stress- and cell death-related markers, the cells treated under different conditions were fixed with cold ethanol (− 20 °C) for 20 min followed by Triton X-100 (0.1%) permeabilization and 10% bovine serum albumin (BSA) blockage. Cells were incubated overnight with primary neural antibodies against choline-acetyltransferase (ChAT, 1:500, cat# AB144 P, Millipore) and vesicular acetylcholine transporter (VAChT, 1:500, cat# SAB4200559, Sigma); primary antibodies against APP751 and/or protein amyloid β1–42 (1:500; clone 6E10 cat# 803014, Biolegend), total TAU (1: 500; t-Tau; cat# T6402, Sigma), and phospho-TAU (p-Tau, 1:500, Ser202/Thr205, cat#MN1020 (AT8), Thermo Fisher Scientific); and primary antibodies against oxidized DJ-1(1:500; ox(Cys106)DJ1; spanning residue C106 of human PARK7/DJ1; oxidized to produce cysteine sulfonic (SO_3) acid; cat # MABN1773, Millipore). To assess cell death, we used primary antibodies against p53-upregulated modulator of apoptosis (1:500; PUMA, cat# ab-9643, Abcam), p53 (1:500; cat# MA5-12-453, Millipore), phospho-c-Jun (1:250; c-Jun (S63/73) cat#sc-16312, Santa Cruz), and caspase-3 (1:250; cat # AB3623, Millipore). After exhaustive rinsing, we incubated the cells with secondary fluorescent antibodies (DyLight 488 and 594 horse anti-rabbit, -goat and -mouse, cat DI 1094, DI 3088, and DI 2488, respectively) at 1:500. The nuclei were stained with 1 µM Hoechst 33,342 (Life Technologies), and images were acquired on a Floyd Cells Imaging Station microscope. The fluorescence intensity was calculated according to[106] using the Image J program (https://imagej.net/)[107].

Analysis of cells.   *Evaluation of intracellular reactive oxygen species (ROS) by fluorescence microscopy.*   To determine the levels of intracellular ROS, we used 2′,7′-dichlorofluorescein diacetate (5 µM, DCFH2-DA; Invitrogen) according to[108]. ChLNs were left in regular culture medium (RCm) for 0, and 4 days. Then, the cells (5×10^3) were incubated with the DCFH2-DA reagent for 30 min at 37 ˚C in the dark. Cells were then washed, and dichlorofluorescein (DCF) fluorescence intensity was determined by analysis of fluorescence microscopy images[109]. The nuclei were stained with 0.5 µM Hoechst 33,342 (2.5 µM) staining compound. The assessment was repeated three times in independent experiments blind to experimenter.

Evaluation of intracellular reactive oxygen species (ROS) by flow cytometry.   ROS was determined with 2′,7′-dichlorofluorescein diacetate (1 µM, DCFH$_2$-DA) according to[108]. ChLNs were left in RCm for 0, and 4 days. Then, the cells (1×10^5) were incubated with DCFH$_2$-DA reagent for 30 min at 37 ˚C in the dark. Cells were then washed, and DCF fluorescence was determined using an LSRFortessa (BD Biosciences). The assessment was repeated 3 times in independent experiments. Quantitative data and figures were obtained using FlowJo7.6.2 Data Analysis Software. The assessment was repeated three times in independent experiments blind to experimenter and flow cytometer analyst[110].

Analysis of mitochondrial membrane potential (ΔΨ$_m$) by fluorescence microscopy.   The ChLNs and CSs were left in RCm for 0, 4 or 11 days, respectively. Then, the cells (5×10^3) were incubated with the passively diffusing and active mitochondria accumulating dye deep red MitoTracker compound (20 nM, final concentration) for 20 min at RT in the dark (Invitrogen, cat # M22426) according to[111]. Cells were then washed twice with PBS. MitoTracker fluorescence intensity was determined by analysis of fluorescence microscopy images. The nuclei were stained with 0.5 µM Hoechst 33,342 (2.5 µM) staining compound. The assessment was repeated three times in independent experiments blind to experimenter and flow cytometer analyst.

Analysis of mitochondrial membrane potential (ΔΨ$_m$) by flow cytometry.   ChLNs were left in RCm for 0, and 4 days. Then, the cells (1×10^5) were incubated for 30 min at RT in the dark with MitoTracker (20 nM, final concentration) according to[111]. The cells were analyzed using an LSRFortessa (BD Biosciences). The experiment was

performed three times in independent experiments, and 10,000 events were acquired for analysis. Quantitative data and figures were obtained using FlowJo 7.6.2 Data Analysis Software. The assessment was repeated three times in independent experiments blind to experimenter and flow cytometer analyst.

Measurement of Aβ1–42 peptide in culture medium. The level of Aβ1–42 peptide was measured according to a previous report[112] with minor modifications. Briefly, WT and PSEN1 I416T ChLNs or CSs were left in RCm for 4 or 11 days, respectively. Then, 100 μl of conditioned medium was collected, and the levels of secreted Aβ1–42 peptides were determined by a solid-phase sandwich ELISA (Invitrogen, Cat# KHB3544) following the manufacturer's instructions. The assessment was repeated three times in independent experiments blind to experimenter.

Intracellular calcium imaging. The cytoplasmic Ca^{2+} concentration ($[Ca^{2+}]_i$) was measured according to ref.[113]. Briefly, ChLNs cultured in *Ch–N-Rm* for 0, and 4 days, and CSs cultured in *Fast-N-spheres medium* for 11 days were transferred to a bath solution (NBS; in mM: 137 NaCl, 5 KCl 2.5 $CaCl_2$, 1 $MgCl_2$, 10 HEPES, pH 7.3, and 22 glucose) containing a Ca^{2+} sensitive indicator (2 μM Fluo3-AM, an acetoxymethyl ester form of the fluorescent dye Fluo-3; Thermo Fisher Scientific Cat F1242) for 30 min at RT and then washed five times. The intracellular Ca^{2+} transients were evoked by acetylcholine (ACh, 1 mM final). Before starting the recordings, several "regions of interest" (ROIs) were defined in the visual field of the camera. One of the ROIs was cell-free, and the fluorescence intensity measured here was considered as "background fluorescence" (F_{bg}). In the "kinetic view" mode, the program calculated and displayed the average fluorescence intensities of the ROIs in arbitrary units (AUs), as the function of time. In the "image view" mode, the time dependence of the spatial distribution of the fluorescence emission was shown, the fluorescence intensities (hence the Ca^{2+} levels) were represented either by pseudocolours. To calculate the changes of the average Ca^{2+}-related fluorescence intensities in the "kinetic view" mode, first the F_{bg} value was determined from the cell-free ROI, then the resting fluorescence intensities (F_{rest}) of the cell-containing ROIs were obtained as the average of the points recorded during a period of 10 s prior to adding ACh. The peaks of the fluorescence transients were found by calculating the average of three consecutive points and identifying those points that gave the highest average value (Fmax). The amplitudes of the Ca^{2+} related fluorescence transients were expressed relative to the resting fluorescence (ΔF/F) and were calculated by the formula $\Delta F/F = (F_{max} - F_{rest})/(F_{rest} - F_{bg})$. The fluorescence intensity was calculated as described by[106] using the Image J program (https://imagej.net/)[107].

Photomicrography and image analysis. Light microscopy photographs and fluorescence microscopy photographs were taken and analyzed exactly as previously reported by[27] using a Zeiss Axiostart 50 Fluorescence Microscope equipped with a Zeiss AxioCam Cm1 and (Zeiss Whlk-Contact-Linsfluoreen, Gmb Schconkirchen, Germany) and Floyd Cells Imaging Station microscope. Mean fluorescence intensity (MFI) was obtained by normalizing total fluorescence to the number of nuclei.

Data analysis. This experimental design was performed exactly as previously reported by[49] based on the statistics considerations described in by[114]. Given that the experimental unit (i.e., the well) data fulfill the independence of observations, the dependent variable is normally distributed in each treatment group (Shapiro–Wilk test), and variances are homogeneous (Levene's test), the statistical significance was determined by Student's t-test, one-way, or two-way ANOVA followed by Bonferroni's or Tukey's post hoc comparison calculated with GraphPad Prism 5.0 software. Differences between groups were only deemed significant when a p-value of < 0.05 (*), < 0.001 (**) and < 0.001 (***). All data are illustrated as the mean ± S.D.

Ethical approval. Menstrual specimen donors provided a signed informed consent approved by the ethics committee of the Sede de Investigación Universitaria (SIU), University of Antioquia, Medellín, Colombia (Act 2020-10854).

Consent to participate. Informed consent was obtained from all individual participants included in the study.

Data availability
All datasets generated for this study are included in the manuscript.

References
1. Wolfe, M. S. *et al.* Two transmembrane aspartates in presenilin-1 required for presenilin endoproteolysis and γ-secretase activity. *Nature* **398**, 513–517. https://doi.org/10.1038/19077 (1999).
2. Khan, A. A., Ali, R. H. & Mirza, B. Evolutionary history of alzheimer disease-causing protein family presenilins with pathological implications. *J. Mol. Evol.* **88**, 674–688. https://doi.org/10.1007/s00239-020-09966-w (2020).
3. Hur, J.-Y. γ-secretase in alzheimer's disease. *Exp. Mol. Med.* **54**, 433–446. https://doi.org/10.1038/s12276-022-00754-8 (2022).
4. Sherrington, R. *et al.* Cloning of a gene bearing missense mutations in early-onset familial Alzheimer's disease. *Nature* **375**, 754–760. https://doi.org/10.1038/375754a0 (1995).
5. Dai, M.-H., Zheng, H., Zeng, L.-D. & Zhang, Y. The genes associated with early-onset Alzheimer's disease. *Oncotarget* **9**, 15132–15143. https://doi.org/10.18632/oncotarget.23738 (2018).

6. Clark, R. F. *et al.* The structure of the presenilin 1 (S182) gene and identification of six novel mutations in early onset AD families. *Nat. Genet.* **11**, 219–222. https://doi.org/10.1038/ng1095-219 (1995).
7. Lalli, M. A. *et al.* Origin of the PSEN1 E280A mutation causing early-onset Alzheimer's disease. *Alzheimer's Dement.* **10**, S277–S283. https://doi.org/10.1016/j.jalz.2013.09.005 (2014).
8. Lopera, F. *et al.* Clinical features of early-onset Alzheimer disease in a large kindred with an E280A presenilin-1 mutation. *JAMA* **277**, 793–799 (1997).
9. Kosik, K. S. *et al.* Homozygosity of the autosomal dominant Alzheimer disease presenilin 1 E280A mutation. *Neurology* **84**, 206–208. https://doi.org/10.1212/WNL.0000000000001130 (2015).
10. Llibre-Guerra, J. J. *et al.* Dominantly inherited alzheimer's disease in Latin America: Genetic heterogeneity and clinical phenotypes. *Alzheimer's Dement.* **17**, 653–664. https://doi.org/10.1002/alz.12227 (2021).
11. Mendivil-Perez, M., Velez-Pardo, C., Kosik, K. S., Lopera, F. & Jimenez-Del-Rio, M. iPSCs-derived nerve-like cells from familial Alzheimer's disease PSEN 1 E280A reveal increased amyloid-beta levels and loss of the Y chromosome. *Neurosci. Lett.* **703**, 111–118. https://doi.org/10.1016/j.neulet.2019.03.032 (2019).
12. Vallejo-Diez, S. *et al.* Generation of one iPSC line (IMEDEAi006-A) from an early-onset familial Alzheimer's Disease (fAD) patient carrying the E280A mutation in the PSEN1 gene. *Stem Cell Res* **37**, 101440. https://doi.org/10.1016/j.scr.2019.101440 (2019).
13. Frederiksen, H. R., Holst, B., Mau-Holzmann, U. A., Freude, K. & Schmid, B. Generation of two isogenic iPSC lines with either a heterozygous or a homozygous E280A mutation in the PSEN1 gene. *Stem Cell Res.* **35**, 101403. https://doi.org/10.1016/j.scr.2019.101403 (2019).
14. Velez-Pardo, C. *et al.* CA1 hippocampal neuronal loss in familial Alzheimer's disease presenilin-1 E280A mutation is related to epilepsy. *Epilepsia* **45**, 751–756. https://doi.org/10.1111/j.0013-9580.2004.55403.x (2004).
15. Dinkel, F. *et al.* Decreased deposition of beta-amyloid 1–38 and increased deposition of beta-amyloid 1–42 in brain tissue of presenilin-1 E280A familial alzheimer's disease patients. *Front. Aging Neurosci.* https://doi.org/10.3389/fnagi.2020.00220 (2020).
16. Arango Lasprilla, J. C., Iglesias, J. & Lopera, F. Neuropsychological stydy of familial Alzheimer's disease caused by mutation E280A in the presenilin 1 gene. *Am. J. Alzheimers Dis. Other Demen.* **18**, 137–146. https://doi.org/10.1177/153331750301800306 (2003).
17. Vannini, P. *et al.* Trajectory of unawareness of memory decline in individuals with autosomal dominant alzheimer disease. *JAMA Netw. Open* **3**, e2027472. https://doi.org/10.1001/jamanetworkopen.2020.27472 (2020).
18. Guzmán-Vélez, E. *et al.* Associative memory and in vivo brain pathology in asymptomatic presenilin-1 E280A carriers. *Neurology* **95**, e1312–e1321. https://doi.org/10.1212/WNL.0000000000010177 (2020).
19. Fox-Fuller, J. T. *et al.* Cortical thickness across the lifespan in a Colombian cohort with autosomal-dominant Alzheimer's disease: A cross-sectional study. *Alzheimer's Dement.: Diagn. Assess. Dis. Monitor.* **13**, e12233. https://doi.org/10.1002/dad2.12233 (2021).
20. Bocanegra, Y. *et al.* Association between visual memory and *In Vivo* amyloid and tau pathology in preclinical autosomal dominant alzheimer's disease. *J. Int. Neuropsychol. Soc.* **27**, 47–55. https://doi.org/10.1017/S1355617720000673 (2021).
21. Armstrong, G. W. *et al.* Retinal imaging findings in carriers with *PSEN1*-associated early-onset familial Alzheimer disease before onset of cognitive symptoms. *JAMA Ophthalmol.* **139**, 49–56. https://doi.org/10.1001/jamaophthalmol.2020.4909 (2021).
22. Palmqvist, S. *et al.* Discriminative accuracy of plasma Phospho-tau217 for Alzheimer disease vs other neurodegenerative disorders. *JAMA* **324**, 772–781. https://doi.org/10.1001/jama.2020.12134 (2020).
23. Quiroz, Y. T. *et al.* Plasma neurofilament light chain in the presenilin 1 E280A autosomal dominant Alzheimer's disease kindred: A cross-sectional and longitudinal cohort study. *Lancet Neurol.* **19**, 513–521. https://doi.org/10.1016/S1474-4422(20)30137-X (2020).
24. Sanchez, J. S. *et al.* Longitudinal amyloid and tau accumulation in autosomal dominant Alzheimer's disease: findings from the Colombia-Boston (COLBOS) biomarker study. *Alzheimers Res. Ther.* **13**, 27. https://doi.org/10.1186/s13195-020-00765-5 (2021).
25. Guzmán-Vélez, E. *et al.* Amyloid-β and tau pathologies relate to distinctive brain dysconnectomics in preclinical autosomal-dominant Alzheimer's disease. *Proc. Natl. Acad. Sci.* **119**, e2113641119. https://doi.org/10.1073/pnas.2113641119 (2022).
26. Tariot, P. N. *et al.* The Alzheimer's Prevention Initiative Autosomal-Dominant Alzheimer's Disease Trial: A study of crenezumab versus placebo in preclinical PSEN1 E280A mutation carriers to evaluate efficacy and safety in the treatment of autosomal-dominant Alzheimer's disease, including a placebo-treated noncarrier cohort. *Alzheimers Dement.* **4**, 150–160. https://doi.org/10.1016/j.trci.2018.02.002 (2018).
27. Soto-Mercado, V., Mendivil-Perez, M., Velez-Pardo, C., Lopera, F. & Jimenez-Del-Rio, M. Cholinergic-like neurons carrying PSEN1 E280A mutation from familial Alzheimer's disease reveal intraneuronal sAPPβ fragments accumulation, hyperphosphorylation of TAU, oxidative stress, apoptosis and Ca²⁺ dysregulation: Therapeutic implications. *PLoS One* **15**, e0221669. https://doi.org/10.1371/journal.pone.0221669 (2020).
28. Soto-Mercado, V., Mendivil-Perez, M., Velez-Pardo, C. & Jimenez-Del-Rio, M. Neuroprotective effect of combined treatment with epigallocatechin 3-gallate and melatonin on familial Alzheimer's disease psen1 E280A cerebral spheroids derived from menstrual mesenchymal stromal cells. *J. Alzheimer's Dis.* **2023**, 1–16. https://doi.org/10.3233/JAD-220903 (2023).
29. Wolfe, M. S. Structure and function of the γ-secretase complex. *Biochemistry* **58**, 2953–2966. https://doi.org/10.1021/acs.biochem.9b00401 (2019).
30. Zhou, R., Yang, G. & Shi, Y. Macromolecular complex in recognition and proteolysis of amyloid precursor protein in Alzheimer's disease. *Curr. Opin. Struct. Biol.* **61**, 1–8. https://doi.org/10.1016/j.sbi.2019.09.004 (2020).
31. Bhattarai, A. *et al.* Mechanism of tripeptide trimming of amyloid β-peptide 49 by γ-secretase. *J. Am. Chem. Soc.* **144**, 6215–6226. https://doi.org/10.1021/jacs.1c10533 (2022).
32. Zhou, R., Yang, G. & Shi, Y. Dominant negative effect of the loss-of-function γ-secretase mutants on the wild-type enzyme through heterooligomerization. *Proc. Natl. Acad. Sci.* **114**, 12731–12736. https://doi.org/10.1073/pnas.1713605114 (2017).
33. Sun, L., Zhou, R., Yang, G. & Shi, Y. Analysis of 138 pathogenic mutations in presenilin-1 on the in vitro production of Aβ42 and Aβ40 peptides by γ-secretase. *Proc. Natl. Acad. Sci.* **114**, E476–E485. https://doi.org/10.1073/pnas.1618657114 (2017).
34. Acosta-Uribe, J. *et al.* A neurodegenerative disease landscape of rare mutations in Colombia due to founder effects. *Genome Med.* **14**, 27. https://doi.org/10.1186/s13073-022-01035-9 (2022).
35. Ramirez Aguilar, L. *et al.* Genetic origin of a large family with a novel *PSEN1* mutation (Ile416Thr). *Alzheimer's Dementia* **15**, 709–719. https://doi.org/10.1016/j.jalz.2018.12.010 (2019).
36. Smith, J. E. In a Colombian Family's Dementia, a Journey Through Race and History. *Undark Magazine* (https://undark.org/) (2019).
37. Fleisher, A. S. *et al.* Florbetapir PET analysis of amyloid-β deposition in the presenilin 1 E280A autosomal dominant Alzheimer's disease kindred: a cross-sectional study. *Lancet Neurol.* **11**, 1057–1065. https://doi.org/10.1016/S1474-4422(12)70227-2 (2012).
38. Quiroz, Y. T. *et al.* Association between amyloid and tau accumulation in young adults with autosomal dominant Alzheimer disease. *JAMA Neurol.* **75**, 548–556. https://doi.org/10.1001/jamaneurol.2017.4907 (2018).
39. Acosta-Baena, N. *et al.* Pre-dementia clinical stages in presenilin 1 E280A familial early-onset Alzheimer's disease: A retrospective cohort study. *Lancet Neurol.* **10**, 213–220. https://doi.org/10.1016/S1474-4422(10)70323-9 (2011).
40. Petit, D. *et al.* Aβ profiles generated by Alzheimer's disease causing PSEN1 variants determine the pathogenicity of the mutation and predict age at disease onset. *Mol. Psychiatry* **27**, 2821–2832. https://doi.org/10.1038/s41380-022-01518-6 (2022).

41. Dominici, M. *et al.* Minimal criteria for defining multipotent mesenchymal stromal cells. The International Society for Cellular Therapy position statement. *Cytotherapy* **8**, 315–317. https://doi.org/10.1080/14653240600855905 (2006).
42. Viswanathan, S. *et al.* Mesenchymal stem versus stromal cells: International Society for Cell & Gene Therapy (ISCT®) mesenchymal stromal cell committee position statement on nomenclature. *Cytotherapy* **21**, 1019–1024. https://doi.org/10.1016/j.jcyt.2019.08.002 (2019).
43. Bozorgmehr, M. *et al.* Endometrial and menstrual blood mesenchymal stem/stromal cells: Biological properties and clinical application. *Front. Cell Dev. Biol.* https://doi.org/10.3389/fcell.2020.00497 (2020).
44. Quintero-Espinosa, D. *et al.* Latent tri-lineage potential of human menstrual blood-derived mesenchymal stromal cells revealed by specific in vitro culture conditions. *Mol. Neurobiol.* **58**, 5194–5209. https://doi.org/10.1007/s12035-021-02442-6 (2021).
45. Lancaster, M. A. & Knoblich, J. A. Generation of cerebral organoids from human pluripotent stem cells. *Nat. Protoc.* **9**, 2329–2340. https://doi.org/10.1038/nprot.2014.158 (2014).
46. Pistollato, F., Canovas-Jorda, D., Zagoura, D. & Price, A. Protocol for the differentiation of human induced pluripotent stem cells into mixed cultures of neurons and glia for neurotoxicity testing. *J. Vis. Exp.* https://doi.org/10.3791/55702 (2017).
47. Rios-Romenets, S. *et al.* Baseline demographic, clinical, and cognitive characteristics of the Alzheimer's prevention initiative (API) autosomal-dominant alzheimer's disease colombia trial. *Alzheimer's Dementia* **16**, 1023–1030. https://doi.org/10.1002/alz.12109 (2020).
48. Soto-Mercado, V., Mendivil-Perez, M., Velez-Pardo, C. & Jimenez-Del-Rio, M. (−)-Epigallocatechin-3-gallate diminishes intra- and extracellular amyloid-induced cytotoxic effects on cholinergic-like neurons from familial Alzheimer's disease PSEN1 E280A. *Biomolecules* **11**, 1845. https://doi.org/10.3390/biom11121845 (2021).
49. Bonilla-Porras, A. R., Velez-Pardo, C. & Jimenez-Del-Rio, M. Fast transdifferentiation of human Wharton's jelly mesenchymal stem cells into neurospheres and nerve-like cells. *J. Neurosci. Methods* **282**, 52–60. https://doi.org/10.1016/j.jneumeth.2017.03.005 (2017).
50. Slanzi, A., Iannoto, G., Rossi, B., Zenaro, E. & Constantin, G. In vitro models of neurodegenerative diseases. *Front. Cell Dev. Biol.* **8**, 328. https://doi.org/10.3389/fcell.2020.00328 (2020).
51. Sharma, N. S., Karan, A., Lee, D., Yan, Z. & Xie, J. Advances in modeling Alzheimer's disease in vitro. *Adv. Nanobiomed. Res.* **1**, 2100097. https://doi.org/10.1002/anbr.202100097 (2021).
52. Hasan, M. F. & Trushina, E. Advances in recapitulating Alzheimer's disease phenotypes using human induced pluripotent stem cell-based in vitro models. *Brain Sci.* **12**, 552. https://doi.org/10.3390/brainsci12050552 (2022).
53. Mendivil-Perez, M., Velez-Pardo, C. & Jimenez-Del-Rio, M. Direct transdifferentiation of human Wharton's jelly mesenchymal stromal cells into cholinergic-like neurons. *J. Neurosci. Methods* **312**, 126–138. https://doi.org/10.1016/j.jneumeth.2018.11.019 (2019).
54. LaFerla, F. M., Green, K. N. & Oddo, S. Intracellular amyloid-β in Alzheimer's disease. *Nat. Rev. Neurosci.* **8**, 499–509. https://doi.org/10.1038/nrn2168 (2007).
55. Welikovitch, L. A. *et al.* Evidence of intraneuronal Aβ accumulation preceding tau pathology in the entorhinal cortex. *Acta Neuropathol.* **136**, 901–917. https://doi.org/10.1007/s00401-018-1922-z (2018).
56. Kondo, T. *et al.* Modeling Alzheimer's disease with iPSCs reveals stress phenotypes associated with intracellular aβ and differential drug responsiveness. *Cell Stem Cell* **12**, 487–496. https://doi.org/10.1016/j.stem.2013.01.009 (2013).
57. Kienlen-Campard, P., Miolet, S., Tasiaux, B. & Octave, J.-N. Intracellular amyloid-β1–42, but not extracellular soluble amyloid-β Peptides, induces neuronal apoptosis. *J. Biol. Chem.* **277**, 15666–15670. https://doi.org/10.1074/jbc.M200887200 (2002).
58. Capetillo-Zarate, E., Gracia, L., Tampellini, D. & Gouras, G. K. Intraneuronal Aβ accumulation, amyloid plaques, and synapse pathology in alzheimer's disease. *Neurodegener. Dis.* **10**, 56–59. https://doi.org/10.1159/000334762 (2012).
59. Brewer, G. J. *et al.* Age-related intraneuronal aggregation of amyloid-β in endosomes, mitochondria, autophagosomes, and lysosomes. *J. Alzheimer's Dis.* **73**, 229–246. https://doi.org/10.3233/JAD-190835 (2020).
60. Dunys, J., Valverde, A. & Checler, F. Are N- and C-terminally truncated Aβ species key pathological triggers in Alzheimer's disease?. *J. Biol. Chem.* **293**, 15419–15428. https://doi.org/10.1074/jbc.R118.003999 (2018).
61. Rostagno, A., Cabrera, E., Lashley, T. & Ghiso, J. N-terminally truncated Aβ4-x proteoforms and their relevance for Alzheimer's pathophysiology. *Transl. Neurodegener.* **11**, 30. https://doi.org/10.1186/s40035-022-00303-3 (2022).
62. Takahashi, R. H., Nagao, T. & Gouras, G. K. Plaque formation and the intraneuronal accumulation of β-amyloid in Alzheimer's disease. *Pathol. Int.* **67**, 185–193. https://doi.org/10.1111/pin.12520 (2017).
63. Cheng, N., Cai, H. & Belluscio, L. In Vivo olfactory model of APP-induced neurodegeneration reveals a reversible cell-autonomous function. *J. Neurosci.* **31**, 13699–13704. https://doi.org/10.1523/JNEUROSCI.1714-11.2011 (2011).
64. Cheng, N., Jiao, S., Gumaste, A., Bai, L. & Belluscio, L. APP overexpression causes aβ-independent neuronal death through intrinsic apoptosis pathway. *eNeuro* **3**, ENEURO.0150-16.2016. https://doi.org/10.1523/ENEURO.0150-16.2016 (2016).
65. Norstrom, E. Metabolic processing of the amyloid precursor protein—New pieces of the Alzheimer's puzzle. *Discov. Med.* **23**, 269–276 (2017).
66. Wolfe, M. S. & Yankner, B. A. Sorting out presenilins in Alzheimer's disease. *Cell* **166**, 13–15. https://doi.org/10.1016/j.cell.2016.06.034 (2016).
67. Fukumori, A., Feilen, L. P. & Steiner, H. Substrate recruitment by γ-secretase. *Semin. Cell Dev. Biol.* **105**, 54–63. https://doi.org/10.1016/j.semcdb.2020.03.006 (2020).
68. Pimenova, A. A. & Goate, A. M. Novel presenilin 1 and 2 double knock-out cell line for in vitro validation of PSEN1 and PSEN2 mutations. *Neurobiol. Dis.* **138**, 104785. https://doi.org/10.1016/j.nbd.2020.104785 (2020).
69. Heilig, E. A., Gutti, U., Tai, T., Shen, J. & Kelleher, R. J. Trans-dominant negative effects of pathogenic PSEN1 mutations on -secretase activity and a production. *J. Neurosci.* **33**, 11606–11617. https://doi.org/10.1523/JNEUROSCI.0954-13.2013 (2013).
70. Sannerud, R. *et al.* Restricted location of PSEN2/γ-secretase determines substrate specificity and generates an intracellular Aβ pool. *Cell* **166**, 193–208. https://doi.org/10.1016/j.cell.2016.05.020 (2016).
71. Wirths, O., Multhaup, G. & Bayer, T. A. A modified beta-amyloid hypothesis: intraneuronal accumulation of the beta-amyloid peptide—The first step of a fatal cascade. *J. Neurochem.* **91**, 513–520. https://doi.org/10.1111/j.1471-4159.2004.02737.x (2004).
72. Kaminsky, Y. G., Tikhonova, L. A. & Kosenko, E. A. Critical analysis of Alzheimer rsquo s amyloid-beta nbsp toxicity to mitochondria. *Front. Biosci.* **20**, 173–197. https://doi.org/10.2741/4304 (2015).
73. Kinumi, T., Kimata, J., Taira, T., Ariga, H. & Niki, E. Cysteine-106 of DJ-1 is the most sensitive cysteine residue to hydrogen peroxide-mediated oxidation in vivo in human umbilical vein endothelial cells. *Biochem. Biophys. Res. Commun.* **317**, 722–728. https://doi.org/10.1016/j.bbrc.2004.03.110 (2004).
74. Marinho, H. S., Real, C., Cyrne, L., Soares, H. & Antunes, F. Hydrogen peroxide sensing, signaling and regulation of transcription factors. *Redox Biol.* **2**, 535–562. https://doi.org/10.1016/j.redox.2014.02.006 (2014).
75. Di Marzo, N., Chisci, E. & Giovannoni, R. The role of hydrogen peroxide in redox-dependent signaling: Homeostatic and pathological responses in mammalian cells. *Cells* **7**, 156. https://doi.org/10.3390/cells7100156 (2018).
76. Rhee, S. G. Redox signaling: Hydrogen peroxide as intracellular messenger. *Exp. Mol. Med.* **31**, 53–59. https://doi.org/10.1038/emm.1999.9 (1999).
77. Cha, M.-Y. *et al.* Mitochondria-specific accumulation of amyloid β induces mitochondrial dysfunction leading to apoptotic cell death. *PLoS One* **7**, e34929. https://doi.org/10.1371/journal.pone.0034929 (2012).

78. Bossy-Wetzel, E., Bakiri, L. & Yaniv, M. Induction of apoptosis by the transcription factor c-Jun. *EMBO J.* **16**, 1695–1709. https://doi.org/10.1093/emboj/16.7.1695 (1997).

79. Aubrey, B. J., Kelly, G. L., Janic, A., Herold, M. J. & Strasser, A. How does p53 induce apoptosis and how does this relate to p53-mediated tumour suppression?. *Cell Death Differ.* **25**, 104–113. https://doi.org/10.1038/cdd.2017.169 (2018).

80. Lu, H., Hou, G., Zhang, Y., Dai, Y. & Zhao, H. c-Jun transactivates Puma gene expression to promote osteoarthritis. *Mol. Med. Rep.* **9**, 1606–1612. https://doi.org/10.3892/mmr.2014.1981 (2014).

81. Yu, J., Zhang, L., Hwang, P. M., Kinzler, K. W. & Vogelstein, B. PUMA induces the rapid apoptosis of colorectal cancer cells. *Mol. Cell* **7**, 673–682. https://doi.org/10.1016/S1097-2765(01)00213-1 (2001).

82. Nakano, K. & Vousden, K. H. PUMA, a Novel Proapoptotic Gene, Is Induced by p53. *Mol. Cell* **7**, 683–694. https://doi.org/10.1016/S1097-2765(01)00214-3 (2001).

83. Li, M. The role of P53 up-regulated modulator of apoptosis (PUMA) in ovarian development, cardiovascular and neurodegenerative diseases. *Apoptosis* **26**, 235–247. https://doi.org/10.1007/s10495-021-01667-z (2021).

84. Obulesu, M. & Lakshmi, M. J. Apoptosis in Alzheimer's disease: An understanding of the physiology. *Pathol. Ther. Avenues. Neurochem Res* **39**, 2301–2312. https://doi.org/10.1007/s11064-014-1454-4 (2014).

85. Yang, J. *et al.* Early pathogenic event of Alzheimer's disease documented in iPSCs from patients with PSEN1 mutations. *Oncotarget* **8**, 7900–7913. https://doi.org/10.18632/oncotarget.13776 (2017).

86. Gallego Villarejo, L. *et al.* Role of intracellular amyloid β as pathway modulator, biomarker, and therapy target. *Int. J. Mol. Sci.* **23**, 4656. https://doi.org/10.3390/ijms23094656 (2022).

87. Huang, L. *et al.* Intracellular amyloid toxicity induces oxytosis/ferroptosis regulated cell death. *Cell Death Dis.* **11**, 828. https://doi.org/10.1038/s41419-020-03020-9 (2020).

88. Lee, J.-H. *et al.* Faulty autolysosome acidification in Alzheimer's disease mouse models induces autophagic build-up of Aβ in neurons, yielding senile plaques. *Nat. Neurosci.* **25**, 688–701. https://doi.org/10.1038/s41593-022-01084-8 (2022).

89. Okazawa, H. Intracellular amyloid hypothesis for ultra-early phase pathology of Alzheimer's disease. *Neuropathology* **41**, 93–98. https://doi.org/10.1111/neup.12738 (2021).

90. Neddens, J. *et al.* Phosphorylation of different tau sites during progression of Alzheimer's disease. *Acta Neuropathol. Commun.* **6**, 52. https://doi.org/10.1186/s40478-018-0557-6 (2018).

91. Alafuzoff, I. *et al.* Staging of neurofibrillary pathology in Alzheimer's disease: A study of the brainnet Europe consortium. *Brain Pathol.* **18**, 484–496. https://doi.org/10.1111/j.1750-3639.2008.00147.x (2008).

92. Neddens, J. *et al.* Correlation of pyroglutamate amyloid β and ptau Ser202/Thr205 levels in Alzheimer's disease and related murine models. *PLoS One* **15**, e0235543. https://doi.org/10.1371/journal.pone.0235543 (2020).

93. Stancu, I.-C., Vasconcelos, B., Terwel, D. & Dewachter, I. Models of β-amyloid induced Tau-pathology: The long and "folded" road to understand the mechanism. *Mol. Neurodegener.* **9**, 51. https://doi.org/10.1186/1750-1326-9-51 (2014).

94. Gomes, L. A. *et al.* Aβ-induced acceleration of Alzheimer-related τ-pathology spreading and its association with prion protein. *Acta Neuropathol.* **138**, 913–941. https://doi.org/10.1007/s00401-019-02053-5 (2019).

95. Ma, Q.-L. *et al.* Amyloid oligomers induce phosphorylation of tau and inactivation of insulin receptor substrate via c-Jun N-terminal kinase signaling: Suppression by omega-3 fatty acids and curcumin. *J. Neurosci.* **29**, 9078–9089. https://doi.org/10.1523/JNEUROSCI.1071-09.2009 (2009).

96. Qin, P. *et al.* Recent advances of small molecule JNK3 inhibitors for Alzheimer's disease. *Bioorg. Chem.* **128**, 106090. https://doi.org/10.1016/j.bioorg.2022.106090 (2022).

97. Kawamoto, E. M., Vivar, C. & Camandola, S. Physiology and pathology of calcium signaling in the brain. *Front. Pharmacol.* https://doi.org/10.3389/fphar.2012.00061 (2012).

98. Tong, B.C.-K., Wu, A. J., Li, M. & Cheung, K.-H. Calcium signaling in Alzheimer's disease & therapies. *Biochim. Biophys. Acta BBA Mol. Cell Res.* **1865**, 1745–1760. https://doi.org/10.1016/j.bbamcr.2018.07.018 (2018).

99. Sawamura, N., Ju, Y. & Asahi, T. Cholinergic receptor, nicotinic, alpha 7 as a target molecule of Arctic mutant amyloid β. *Neural. Regen. Res.* **13**, 1360–1361. https://doi.org/10.4103/1673-5374.235238 (2018).

100. Dani, J. A. & Bertrand, D. Nicotinic acetylcholine receptors and nicotinic cholinergic mechanisms of the central nervous system. *Annu. Rev. Pharmacol. Toxicol.* **47**, 699–729. https://doi.org/10.1146/annurev.pharmtox.47.120505.105214 (2007).

101. Yiannopoulou, K. G., Anastasiou, A. I., Zachariou, V. & Pelidou, S.-H. Reasons for failed trials of disease-modifying treatments for alzheimer disease and their contribution in recent research. *Biomedicines* **7**, 97. https://doi.org/10.3390/biomedicines7040097 (2019).

102. Imbimbo, B. P., Lucca, U. & Watling, M. Can anti–B-amyloid monoclonal antibodies work in autosomal dominant alzheimer disease?. *Neurol. Genet.* **7**, e535. https://doi.org/10.1212/NXG.0000000000000535 (2021).

103. Liu, Y. *et al.* Biological characteristics of human menstrual blood-derived endometrial stem cells. *J. Cell Mol. Med.* **22**, 1627–1639. https://doi.org/10.1111/jcmm.13437 (2018).

104. Huang, S. *et al.* Dissimilar characteristics of umbilical cord mesenchymal stem cells from donors of different ages. *Cell Tissue Bank* **14**, 707–713. https://doi.org/10.1007/s10561-013-9364-2 (2013).

105. Xie, X. *et al.* Construction of engineered corpus cavernosum with primary mesenchymal stem cells in vitro. *Sci. Rep.* **7**, 18053. https://doi.org/10.1038/s41598-017-18129-9 (2017).

106. Jensen, E. C. Quantitative analysis of histological staining and fluorescence using imageJ. *Anat. Rec.* **296**, 378–381. https://doi.org/10.1002/ar.22641 (2013).

107. Schindelin, J. *et al.* Fiji: An open-source platform for biological-image analysis. *Nat. Methods* **9**, 676–682. https://doi.org/10.1038/nmeth.2019 (2012).

108. Siddiqui, M. A. *et al.* Rotenone-induced oxidative stress and apoptosis in human liver HepG2 cells. *Mol. Cell Biochem.* **384**, 59–69. https://doi.org/10.1007/s11010-013-1781-9 (2013).

109. Lichtman, J. W. & Conchello, J.-A. Fluorescence microscopy. *Nat. Methods* **2**, 910–919. https://doi.org/10.1038/nmeth817 (2005).

110. Adan, A., Alizada, G., Kiraz, Y., Baran, Y. & Nalbant, A. Flow cytometry: Basic principles and applications. *Crit. Rev. Biotechnol.* **37**, 163–176. https://doi.org/10.3109/07388551.2015.1128876 (2017).

111. Arcila, M. L. *et al.* Activation of apoptosis, but not necrosis, during Mycobacterium tuberculosis infection correlated with decreased bacterial growth: Role of TNF-α, IL-10, caspases and phospholipase A2. *Cell Immunol.* **249**, 80–93. https://doi.org/10.1016/j.cellimm.2007.11.006 (2007).

112. Armijo, E. *et al.* Increased susceptibility to Aβ toxicity in neuronal cultures derived from familial Alzheimer's disease (PSEN1-A246E) induced pluripotent stem cells. *Neurosci. Lett.* **639**, 74–81. https://doi.org/10.1016/j.neulet.2016.12.060 (2017).

113. Pap, P., Kőszeghy, Á., Szűcs, G. & Rusznák, Z. Cytoplasmic Ca^{2+} concentration changes evoked by cholinergic stimulation in primary astrocyte cultures prepared from the rat cochlear nucleus. *Hear. Res.* **255**, 73–83. https://doi.org/10.1016/j.heares.2009.05.006 (2009).

114. Lazic, S. E., Clarke-Williams, C. J. & Munafò, M. R. What exactly is 'N' in cell culture and animal experiments?. *PLoS Biol.* **16**, e2005282. https://doi.org/10.1371/journal.pbio.2005282 (2018).

Author contributions

Conceptualization M.J.-Del-R., C. V.-P.; Methodology N. G.-S., M. M.-P., C. V.-P.; Validation N. G.-S., M. M.-P.; Formal analysis N. G.-S., M. M.-P.; Investigation N. G.-S., M. M.-P., F.L.; Data curation N. G.-S., M. M.-P.; Supervision M.J.-Del-R.; Project administration C. V.-P.; Resources F.L., C. V.-P., M.J.-Del-R.; Funding acquisition M.J.-Del-R., C. V.-P.; Writing—original draft preparation M.J.-Del-R., C. V.-P.; Writing—review and editing N. G.-S., M. M.-P., M.J.-Del-R., F.L., C. V.-P.

Funding

Competing interests

The authors declare no competing interests.

Additional information

Supplementary Information The online version contains supplementary material available at https://doi.org/10.1038/s41598-023-39630-4.

Correspondence and requests for materials should be addressed to C.V.-P.

Reprints and permissions information is available at www.nature.com/reprints.

Publisher's note Springer Nature remains neutral with regard to jurisdictional claims in published maps and institutional affiliations.